



HAL
open science

Parvimonas micra , an oral pathobiont associated with colorectal cancer, epigenetically reprograms human primary intestinal epithelial cells

Emma Bergsten, Denis Mestivier, Francoise Donnadiou, Thierry Pedron, Landry Tsoumtsas, Emmanuel Lemichez, Olivier Gorgette, Stevann Volant, Abiba Doukani, Philippe Sansonetti, et al.

► To cite this version:

Emma Bergsten, Denis Mestivier, Francoise Donnadiou, Thierry Pedron, Landry Tsoumtsas, et al.. Parvimonas micra , an oral pathobiont associated with colorectal cancer, epigenetically reprograms human primary intestinal epithelial cells. 2022. pasteur-03689065

HAL Id: pasteur-03689065

<https://pasteur.hal.science/pasteur-03689065>

Preprint submitted on 6 Jun 2022

HAL is a multi-disciplinary open access archive for the deposit and dissemination of scientific research documents, whether they are published or not. The documents may come from teaching and research institutions in France or abroad, or from public or private research centers.

L'archive ouverte pluridisciplinaire **HAL**, est destinée au dépôt et à la diffusion de documents scientifiques de niveau recherche, publiés ou non, émanant des établissements d'enseignement et de recherche français ou étrangers, des laboratoires publics ou privés.



Distributed under a Creative Commons Attribution 4.0 International License

1 ***Parvimonas micra*, an oral pathobiont associated** 2 **with colorectal cancer, epigenetically reprograms** 3 **human primary intestinal epithelial cells**

4
5 Emma Bergsten,^{1,2,4} Denis Mestivier,^{2,3} Françoise Donnadieu,¹ Thierry Pedron,^{1,10} Landry Tsoumtsas,⁴
6 Emmanuel Lemichez,⁴ Olivier Gorgette,⁶ Stevonn Volant,⁷ Abiba Doukani,⁸ Philippe J. Sansonetti,^{1,9,*}
7 Iradj Sobhani,^{2,5,*} and Giulia Nigro^{1,11,*,#}

8 **Authors/affiliations**

9 ¹ Unité de Pathogénie Microbienne Moléculaire, INSERM U1202, Institut Pasteur, Paris 75015, France.

10 ² Équipe universitaire EC2M3-EA7375, Université Paris- Est (UPEC), Créteil 94000, France.

11 ³ Plateforme de Bio-informatique, Institut Mondor de Recherche Biomédicale (IMRB / INSERM U955), Université
12 Paris-Est, Créteil 94000 France.

13 ⁴ Unité des Toxines Bactériennes, CNRS UMR2001, INSERM U1306, Institut Pasteur, Paris 75015, France.

14 ⁵ Service de Gastroentérologie, CHU Henri Mondor APHP, Créteil 94000, France.

15 ⁶ Unité de bio-imagerie ultra-structurale (UtechS UBI), Centre de Recherche et de Ressources Technologies (C2RT),
16 Institut Pasteur, Paris 75015, France.

17 ⁷ Bioinformatics and Biostatistics Hub, Institut Pasteur, Paris 75015, France.

18 ⁸ Sorbonne Université, Inserm, Unité Mixte de Service Production et Analyse de données en Sciences de la Vie et
19 en Santé, UMS PASS, Plateforme P3S, F-75005, Paris, France.

20 ⁹ Chaire de Microbiologie et Maladies Infectieuses, Collège de France, 75231 Paris, France.

21 ¹⁰ Present address: Unité Bactériophage, Bactérie, Hôte, Institut Pasteur, Paris 75015, France.

22 ¹¹ Present address: Microenvironment and Immunity Unit, INSERM U1224, Institut Pasteur, Paris 75015, France.

23 * Correspondence: philippe.sansonetti@pasteur.fr, iradj.sobhani@aphp.fr, giulia.nigro@pasteur.fr

24 # Lead contact

25

26 **Summary**

27 Recently, an intestinal dysbiotic microbiota in the feces of colorectal cancer (CRC) patients with an
28 enrichment of bacteria belonging to the oral microbiota has been described. Here we characterized and
29 investigated one of these oral pathobionts, the Gram-positive anaerobic coccus *Parvimonas micra*. We
30 identified two phylotypes (A and B) exhibiting different phenotypes and adhesion capabilities. We
31 observed a strong association of phylotype A with CRC, with its higher abundance in feces and in tumoral
32 tissue compared to the normal homologous colonic mucosa, which was associated with a distinct
33 methylation status of patients. By developing an *in vitro* hypoxic co-culture system of human primary
34 colonic cells with anaerobic bacteria, we showed that *P. micra* phylotype A induces modifications in DNA

35 methylation of the promoters of several tumor-suppressor genes, oncogenes, and genes involved in
36 epithelial-mesenchymal transition, providing evidence of its possible role in carcinogenesis.

37

38 **Keywords:** Colorectal cancer, colonic epithelial primary cells, Dysbiosis, *Parvimonas micra*, DNA
39 methylation.

40

41 **Introduction**

42 Colorectal cancer (CRC) is a multifactorial disease due to various genetic and environmental factors that
43 contribute to tumor formation and disease development. Genetic predispositions for CRC, such as Lynch
44 syndrome (also called human no polyposis colonic cancer-HNPCC) or familial adenomatous polyposis
45 (FAP), only accounts for a minority of CRC, representing less than 5% of all cases (Jiao et al., 2014). The
46 overwhelming majority of CRCs are sporadic cancers, i.e., the cause is unknown. Several lifestyle
47 environmental factors increase the risk of CRC including physical inactivity (Samad et al., 2005),
48 overweight (Kyrgiou et al., 2017) and high consumption of red meat, processed meat and unsaturated
49 fatty acids (Chan et al., 2011). The identification of lifestyle factors supports the hypothesis that the
50 increase in CRC incidence is strictly related to environmental changes. Among environmental factors, the
51 role of microorganisms in cancer has been increasingly recognized and a global imbalance, called
52 dysbiosis, of gut microbiota compared to healthy individuals was observed in several cancers such as
53 biliary, hepatic, breast cancers, or CRC (Schwabe and Jobin, 2013). Thus, the gut microbiota has
54 emerged as an important carcinogenic environmental factor, in particular for CRC, due to the gut
55 microbiota proximity and constant crosstalk with the intestinal epithelium (Soderholm and Pedicord,
56 2019). Different bacterial species, for example *Bacteroides fragilis*, *Fusobacterium nucleatum* (*F.*
57 *nucleatum*), pathogenic strains of *Escherichia coli*, or *Streptococcus gallolyticus*, have been associated
58 with CRC development and mechanistic studies have tried understand the roles of these bacteria in
59 carcinogenesis (Goodwin et al., 2011; Pasquereau-Kotula et al., 2018; Pleguezuelos-Manzano et al.,
60 2020; Rubinstein et al., 2013). Recently, our team and others have identified, by metagenomic studies
61 from humans' feces, not only the intestinal bacterium *F. nucleatum* associated with CRC but also bacteria
62 belonging to the oral microbiota, such as *Gemella morbillorum*, *Solobacterium moorei*, *Porphyromonas*
63 *gingivalis*, and *Parvimonas micra* (*P. micra*) (Koliarakis et al., 2019; Schmidt et al., 2019; Sobhani et al.,

64 2019). The overabundance of these bacteria in the colonic niche may be an etiological factor in CRC
65 (Saffarian et al., 2019), but the underlying mechanisms remain to be elucidated. Here, we chose to focus
66 on the candidate bacterium, *P. micra*.

67 *P. micra*, the only described species within its genus, is a Gram-positive anaerobic coccus and
68 commensal of the oral cavity (Rams et al., 1992). *P. micra* could be considered a pathobiont (Kamada et
69 al., 2013) because it is often isolated from oral polymicrobial infections associated with periodontitis
70 (Socransky et al., 1999), from superficial polymicrobial infections, including wounds, ulcers, and skin
71 abscesses (Bowler and Davies, 1999b, 1999a; Edmiston et al., 1990; Mousa, 1997; Sanderson et al.,
72 1979), as well as from deep tissue infections in the brain, lung and reproductive organs (Murdoch et al.,
73 1988).

74 *P. micra* has been poorly studied due to difficulties in its cultivation and laboratory identification by
75 traditional methods and the polymicrobial nature of the infective zones from which it is usually isolated.
76 The aim of this work was to better characterize *P. micra*, define its carriage in CRC patients, and analyze
77 *in vitro* the nature of the crosstalk between this oral pathobiont and colonic epithelial cells. We identified
78 two phylotypes of *P. micra* (A and B) and found that phylotype A is strongly associated with human CRC,
79 and particularly in patients with a positive cumulative methylation index, and *in vitro* induces DNA
80 methylation modifications in colonic primary epithelial cells.

81

82 **Results**

83 ***P. micra* exists in two phylotypes with phenotypic and genetic diversity**

84 To explore *P. micra* diversity, twenty-seven clinical isolates from various types of infections (blood,
85 systemic, and oral cavity) were collected (Table S1), while, unfortunately, the high bacterial diversity in
86 feces precluded *P. micra* isolation from CRC patient fecal samples. *P. micra* colonies on blood agar plates
87 appeared heterogeneous. A contact haemolytic activity was observed in twenty isolates (20/27) (Figure
88 1A, Figure S1A) while *P. micra* colonies from solid agar plates were found to be either “compact” (7/27)
89 or “non-compact” (20/27) (Figure 1A, Figure S1A). Sedimentation assays in liquid of two representative
90 isolates: ATCC 33270 (“non-compact”) and HHM B1Na17 (“compact”), (named hereafter *PmA* and *PmB*,
91 respectively), showed differences in the aggregation rate (Figure S1B).

92 Phenotypical differences observed among the twenty-seven isolates could reflect genetic diversity.
93 Indeed, sequencing of the full 16S rDNA of these isolates revealed two distinct phylogenetic groups: A
94 and B (Figure 1A). *Finegoldia magna* (*F. magna*), the most closely related bacterial species to *P. micra*,
95 was used to set the root of the phylogenetic tree. Interestingly, all *P. micra* isolates from phylotype A were
96 haemolytic whereas isolates belonging to phylotype B were not. Likewise, most phylotype B isolates were
97 “compact” whereas phylotype A isolates were not. To deepen our analysis, the ten *P. micra* genomes
98 available on the NCBI database were clustered based on the presence/absence of genes. Grouping of
99 isolates confirmed the existence of phylotypes A and B (Figure S1C).

100 Recent clinical studies using 16S rDNA sequencing from tissue had shown the presence of *Parvimonas*
101 sequences in tumoral and normal homologous colonic mucosa of CRC patients, suggesting that this
102 microorganism may be able to adhere to colonocytes or the colonic cellular matrix (Flemer et al., 2017;
103 Gao et al., 2017). We therefore measured the ability a representative isolate from each phylotype, *PmA*
104 (phylotype A) and *PmB* (phylotype B), to adhere to different extracellular matrix (ECM) proteins and three
105 human colonic cell lines. *PmA* adhered to the ECM proteins collagen I, collagen IV, fibronectin and
106 laminin, as well as to Matrigel® but not to fibrinogen, whereas *PmB* did not adhere to any of these ECM
107 proteins (Figure 1B). Similarly, *PmA* adhered 6-, 2-, and 3-fold more to Caco-2, HT-29, and HCT116,
108 respectively as compared to *PmB* ($p < 0.05$) (Figure 1C), indicating heterogeneity of adhesion capacity in
109 *P. micra* phylotypes.

110 To explore whether differences in the aggregation phenotype could be due to specific bacterial surface
111 structures, ultrathin sections of the two phylotypes were analyzed by positive contrast transmission
112 electron microscopy. Spiky surface structures were observed only in *PmB* (non haemolytic, “compact”)
113 and not in *PmA* (haemolytic, “non-compact”) (Figure 1D).

114 These data show that two phenotypically and genetically different phylotypes can be described for *P.*
115 *micra*.

116

117 ***P. micra* phylotype A is associated with CRC**

118 Differences in the *in vitro* adhesion capacity of the two phylotypes might reflect a different colonization
119 ability *in vivo*. To assess this hypothesis, we first improved the resolution of our whole genome
120 sequencing (WGS) metagenomic analysis of the *P. micra* sequences carried in CRC patients’ feces

121 (Zeller et al., 2014) focusing on the taxonomic assignment of raw data in order to precisely investigate
122 microbial composition.

123 We observed an enrichment (27% versus 1.1%) of *P. micra* in the feces of CRC patients compared to
124 control healthy individuals. Three taxa of *P. micra* were detected: '*Parvimonas micra*' from phylotype A,
125 and '*Parvimonas* sp. oral taxon 393 - F0440' and '*Parvimonas* sp. oral taxon 110 - F0139' from phylotype
126 B. All 27% of *Parvimonas* positive patients carried the phylotype A in their feces, except in one patient
127 where reads of both phylotypes were detected.

128 We then analyzed *Parvimonas* carriage in feces of CRC patients and control individuals, as well as from
129 paired tumor and normal homologous tissues (adjacent to the tumor), using 16S rDNA sequencing of the
130 V3-V4 region. As expected, the occurrence of *Parvimonas* in feces was enriched in CRC patients (81%)
131 as compared to control individuals (60%) (Figure 2A), while *Parvimonas* carriage increased at early
132 stages of CRC (I & II) according to TNM (tumor-node-metastasis) staging of CRC (Figure 2A), an
133 observation consistent with previous WGS results. In 78% of CRC patients, *Parvimonas* sequences were
134 detected in both tumoral and normal homologous samples with a significant enrichment of the bacterium
135 in the tumoral tissues (means of 2.2% versus 0.53% respectively; $p < 0.01$) (Figure 2B). Prevalence of
136 *Parvimonas* in tissues showed no difference according to the TNM staging, with 74% in stages I-II versus
137 84% in stages III-IV and a respective abundance of 1.34% and 1.41% (Figure 2B).

138 The V3-V4 regions of the 16S rDNA was then analyzed to discriminate between *Parvimonas* phylotypes
139 A and B. Forty-four percent of control individuals carried the phylotype A in their feces compared to 61%
140 of the CRC patients ($p < 0.01$), whereas no difference in the prevalence of the phylotype B was observed
141 (22% and 27%, respectively) (Figure 2C). An increase in the abundance of the phylotype A, but not of
142 the phylotype B, was also observed in tumor tissues compared to homologous normal tissues ($p < 0.05$)
143 (Figure 2D).

144 Previously, we demonstrated a strong correlation between *Parvimonas micra* carriage in feces and a
145 positive cumulative methylation index (CMI) in the blood based on the methylation levels of promoters in
146 the WIF1 gene involved in carcinogenesis and PENK, and NPY, two neuromediators genes (Sobhani et
147 al., 2019). Thus, we wondered whether the phylotypes herein described, were correlated with the CMI.
148 Analysis of 16S rDNA sequencing data from feces showed that phylotype A was correlated with a positive
149 CMI ($p < 0.01$) but this was not the case for phylotype B (Figure 2E). *Parvimonas* carriage in tissues was

150 also correlated with a positive CMI ($p < 0.05$), although the number of samples was not sufficient to
151 discriminate between the two phylotypes (Figure 2F).

152 These results indicate that *Parvimonas micra* phylotype A sub-species is associated with CRC.

153

154 ***P. micra* impact on human colonic primary epithelial cells**

155 Colorectal tumor is defined as a group of anarchically proliferating cells with DNA mutations and aberrant
156 DNA methylation. To determine whether *P. micra* has an impact on host cells, we first developed a
157 compatible co-culture model between this oxygen-sensitive anaerobic microorganism and primary human
158 colonic epithelial cells. Colonic samples were obtained from normal site (far from tumor tissue) of two
159 colonic tumor resections. Colonic crypts were isolated and cultured as organoids (Figure 3A), allowing
160 amplification of initial material through stem cell proliferation. To develop a system where bacteria could
161 be in contact with the apical pole of primary cells, reflecting a physiological situation, organoid fragments
162 were seeded onto a Transwell® insert system and grown to confluency up to a polarized monolayer
163 (Figure 3B), as previously described (Noel et al., 2017). Cell growth and formation of a tight monolayer
164 were monitored over time by phase-contrast microscopy and transepithelial electrical resistance (TEER)
165 measurements (Figures 3C and D). Under these culture conditions, monolayers were fully confluent three
166 days after organoids fragments were seeded on the inserts (Figure 3D).

167 *P. micra* has been described as an anaerobic microorganism (Kremer et al., 1997) and little is known
168 about its oxygen tolerance. To determine compatible oxygenation conditions with eukaryotic cell growth
169 requirements, *P. micra* was cultivated at various oxygen concentrations (0, 2, or 21% O₂) and viability
170 was assessed by Colony Forming Units (CFU) counting at different time points. *P. micra*'s viability
171 dropped by 70% in less than ten minutes in aerobic conditions (21% O₂), whereas in hypoxic conditions
172 (2% O₂) it was able to grow albeit at half the rate compared to full anaerobic conditions (Figure S2A).
173 Thus, primary cells were grown for four days in aerobic conditions to allow monolayer formation, followed
174 by three days in hypoxia (2% O₂). The primary cell monolayer's integrity was maintained in these
175 conditions (Figures 3C and D) and showed all characteristics of a differentiated epithelium as assessed
176 by the presence of tight junctions, differentiated epithelial cells, colonocytes, goblet cells, and
177 enteroendocrine cells (Figure 3E).

178 To investigate the possible involvement of *P. micra* in early oncogenic processes, we co-cultivated
179 primary cell monolayers with the two reference isolates, *PmA* and *PmB*, as well as *F. magna*, which is
180 the closest phylogenetic taxon to *P. micra*, as a control. One day prior to co-culture, cells were placed in
181 hypoxic conditions (2% O₂) to allow pre-adaptation. On the fourth day of the culture, cells were co-cultured
182 with bacteria using a multiplicity of infection (M.O.I.) of 250 and incubated at 2% hypoxic conditions for
183 48 hours prior to analysis (Figure 3F). Bacterial growth was monitored over time by CFU counting of co-
184 culture supernatants. After 48 hours of co-culture, *PmA* showed a 5-fold increase but did not impact cell
185 viability, while *PmB* and *F. magna* showed no significant growth but had a more toxic effect, inducing a
186 30% decrease in cell viability (Figure 3G). Cell proliferation was measured by Ki-67 quantification upon
187 immunofluorescent staining and no significant differences were observed between the various groups
188 (Figure S2C, F). Because goblet cells are known to be impacted by intestinal microbes (Deplancke and
189 Gaskins, 2001), we quantified their proportion and no significant differences were observed (Figure S2D,
190 G). Moreover, because virulent bacteria can stimulate NF- κ B and induce DNA breaks (Nougayrède et
191 al., 2006) the proportion of cells with DNA double-strand breaks was measured and was found unchanged
192 (Figure S2E, H). Yet, as compared to the NS condition, a significant increase in nuclear NF- κ B was
193 observed with both *PmA* ($p < 0.01$) and *PmB* ($p < 0.05$), but not *F. magna*, (Figure 3H). Thus, in the time
194 frame of the experiments, *P. micra* did not induce DNA breaks despite activation of the NF- κ B pathway
195 and the possible induction of an inflammatory program in exposed cells. These results suggested that *P.*
196 *micra* might contribute to host epithelial cell mutagenesis through a NF- κ B pathway-mediated epigenetic
197 effect.

198

199 ***P. micra* phylotype A induces DNA methylation changes**

200 Global DNA methylation was measured using a 5-methyl-cytosine dosage assay. *In vitro* co-cultures of
201 both *P. micra* phylotypes showed a significant increase in global DNA methylation of primary cells as
202 compared to NS condition ($p < 0.05$) or to *F. magna* (Figure 4A). To identify affected genes, a genome-
203 wide DNA methylation analysis was performed on the human colonic primary cells exposed or not to *P.*
204 *micra* phylotypes or *F. magna*, using the Infinium MethylationEPIC BeadChip from Illumina. The
205 methylation status of >850,000 CpG sites was assessed at all colonocyte genome targeting sites already
206 known to be methylation-sensitive (Data set ready on Mendeley Data with the following DOI:

207 10.17632/nwj3bgbg5m.1). These were then classified by context (in or outside of CpG islands) and
208 regions: body genes (3' or 5' UTR, first exon, exon bond, and body), promoters (200 or 1500 bases
209 upstream of the transcriptional start site [TSS200 and TSS1500]) or intergenic. Using the LIMMA paired
210 test we identified hyper- and hypo-methylated CpG sites from colonic primary cells challenged with
211 bacteria compared to non-stimulated cells. CpG sites were then sorted into four categories: CpGs in
212 promoters and within CpG islands; CpGs in promoters and outside CpG islands; CpGs in body genes
213 (promoters region excluded) and within CpG islands; as well as CpGs in body genes outside of CpG
214 islands. Because aberrant DNA methylation in promoters of tumor suppressor genes (TSGs) is a hallmark
215 of CRC, combined p-values of differentially methylated CpG sites within the same gene were determined
216 based on these four categories. We found that DNA methylation modifications were induced by all three
217 bacteria while *PmB* promoted the highest number of hypo- or hyper-methylated genes (Figure 4B and
218 C). Focusing on CpGs located in promoters and within CpG islands, we identified 15, 90, and 39
219 differentially methylated genes between non-stimulated cells as compared to cells co-cultivated with
220 *PmA*, *PmB*, and *F. magna*, respectively. Venn diagram revealed six genes in common between *PmB* and
221 *F. magna*, only one in-between the two phylotypes of *P. micra*, and two genes for *PmA* and *F. magna*
222 (Figure 4D). Strikingly, 60% of the modified genes were either oncogenes, tumor suppressor genes, or
223 genes involved in epithelial-mesenchymal transition (EMT), for *PmA* versus only 10% for *PmB* and 18%
224 for *F. magna* (Figure 4E). In addition, cells co-cultivated with *PmA* presented hyper-methylation of several
225 tumor suppressor gene promoters such as SCIN, HACE1, TSPAN13, FBXO32, IGFBP7, SIX1 or CXXC5.
226 Except for the KIAA0494 gene that codes for an uncharacterized protein, all of the genes with a
227 modification of the methylation status of their promoters induced by *PmA* are involved in carcinogenesis,
228 particularly in EMT processes (Table S3) or cytoskeleton remodeling. These results suggest that *P. micra*
229 phylotype A induces modifications in the expression of a specific gene set through the selective epigenetic
230 modulation of gene promoters among which we identified well-characterized carcinogenesis regulators.

231

232 **Discussion**

233 Recently, we and others observed an epidemiological association between colorectal cancer and several
234 oral bacteria such as *F. nucleatum*, *Porphyromonas gingivalis*, *Solobacterium moorei*,
235 *Peptostreptococcus stomatis*, *Gemella morbillorum*, and *P. micra*, through 16S rDNA sequencing (Baxter

236 et al., 2014; Flemer et al., 2017) or metagenome analysis (Yu et al., 2017; Schmidt et al., 2019; Sobhani
237 et al., 2019), of fecal samples. Some of these oral bacteria were also associated with colonic tissues of
238 CRC patients (Gao et al., 2015; Nakatsu et al., 2015; Flemer et al., 2017), where they were more
239 abundant in tumors than in adjacent healthy tissues (Nakatsu et al., 2015; Gao et al., 2017). In the present
240 study, we focused on *P. micra*, at the subspecies level, and quantitatively measured its carriage in feces
241 and in association with colonic tissues in a large cohort from Henri Mondor hospital (Directed by Prof. I.
242 Sobhani) that includes normal colonoscopy, adenomatous and CRC patients. We observed, as others
243 have (Xu et al., 2020), that *P. micra* is enriched in CRC from early stages (I and II of TNM classification),
244 but not in feces of patients with adenomas, benign tumors considered as precursor of CRC (Fearon and
245 Vogelstein, 1990). Since *P. micra* sequences were associated with adenoma tissues, we hypothesized
246 that *P. micra* could be involved in the early steps of colon carcinogenesis. If *P. micra* is involved in
247 promoting and/or accelerating carcinogenesis, *P. micra*, a common habitant of the oral cavity, would also
248 have to be adapted for growth in the carcinogenesis-modified gut microenvironment. Indeed, oral
249 microbiota such as *P. micra*, *F. nucleatum*, *P. stomatis*, and *G. morbilorum* were observed in biofilms-like
250 structures on colonic mucosa of CRC patients and healthy subjects, (Dejea and Sears, 2016; Dejea et
251 al., 2014; Drewes et al., 2017) that could be a way for these pathobionts to colonize the colonic mucosa
252 (Horiuchi et al., 2020; Koliarakis et al., 2019; Li et al., 2017).

253 A recent *in vivo* study reported that *Apc*^{Min/+} mice orally gavaged with *P. micra* exhibited a significantly
254 higher tumor burden and were associated with altered immune responses and enhanced inflammation
255 (Zhao et al., 2020). However, the mechanisms and the bacterial factors involved remain unknown. To
256 move from association to causality, the first step is to select the most relevant genotype/phylogroup
257 associated with CRC and to develop *in vitro* models to assess the interaction of *P. micra* with host cells.
258 Here we succeeded in developing a physiologically-relevant, low-oxygen *in vitro* co-culturing model of
259 bacteria with primary human colonic intestinal cells to assess the effect of *P. micra* on colonic cells. Using
260 this novel methodology, we established an epidemiological association of *P. micra* phylotype A with CRC.
261 Notably, this cutting-edge cellular model offers a novel means to interrogate the effects of similar other
262 pathobionts on colonocytes. Using this novel methodology, no impact of *P. micra* was observed on cell
263 proliferation or differentiation, nor detected significant DNA damaging capacity. In contrast, *P. micra* co-
264 culture induced the activation of the central transcription factor NF- κ B, a key modulator of inflammation

265 and immune responses known to be constitutively activated in most cancers. Congruent with this
266 observation, *P. micra*, like other oral pathobionts, have been shown to be associated with the CMS1
267 subtype of CRC, which makes up 14% of all CRC cases (Purcell et al., 2017), and with an over-activation
268 of genes involved in immune responses. The CMS1 tumors, also called “immune subtype”, are
269 characterized by a strong immune cell infiltration of CD8+ cytotoxic T cells, CD4+ T helper cells, and
270 natural killer cells (Becht et al., 2016; Guinney et al., 2015). *P. micra* and inflammatory responses
271 therefore seem to be key aspects in colon carcinogenesis.

272 Apart from specific mutations that characterize cancerous cells, epigenetic modifications of DNA and
273 methylation of tumor suppressor genes (TSGs) promoters are essential in colonic carcinogenesis. We
274 recently showed that CRC-associated dysbiotic feces transplanted to mice caused epigenetic changes
275 similar to those observed in human tumors and the occurrence of murine colonic crypt aberrations
276 (Sobhani et al., 2019). Furthermore, the CMS1 CRC subtype, in which *P. micra* and other oral bacteria
277 enrichment has been observed (Purcell et al., 2017), is associated with the phenotype of
278 hypermethylation of CpG islands in tumor suppressor gene promoters (high CIMP) (Guinney et al., 2015).
279 Consistent with this hypothesis, Xia *et al.* observed an associations between enrichments of *F. nucleatum*
280 or *Parvimonas spp.* and promoter methylation of several TSGs in tumoral tissue, (Xia et al., 2020),
281 although they did not focus on *Parvimonas* subspecies. It is therefore tempting to speculate that *P. micra*
282 might have a similar driver role in CRC by inducing hypermethylation in the promoter regions of keys
283 TSGs.

284 In the present study, we report for the first time that *P. micra* increased global DNA methylation of target
285 host cells using an *in vitro* co-culture model of human primary colonic cells. Notably, by comparing
286 different *P. micra* phylotypes, we established a *P. micra* phylotype A-dependent signature of methylated
287 promoters whose gene function converges towards the regulation of the cytoskeleton (Table S3) and
288 include TSGs or genes involved in epithelial-mesenchymal transition (EMT) (Table S3). For example,
289 Scinderin gene (SCIN) coding for a Ca²⁺-dependent actin-severing and capping protein, is involved in the
290 regulation of actin cytoskeleton and known to be overexpressed in CRC (Lin et al., 2019); Tetraspanin
291 13 (TSPAN13) is a tumor suppressor gene coding for a transmembrane signal transduction protein that
292 regulates cell development, motility, and invasion (Lou et al., 2017); DIAPH3 gene, is a major regulator
293 of actin cytoskeleton involved in cell mobility and adhesion (Rana et al., 2018); Semaphorin 3F

294 (SEMA3F), is a tumor suppressor gene coding a secreted protein involved in cytoskeletal collapse and
295 loss of migration (Shimizu et al., 2008); and SASH1 is a TSG coding for a scaffold protein involved in the
296 TLR4 signaling, and known to interact with the actin cytoskeleton to maintain stable cell-cell adhesion
297 (Martini et al., 2011). Notably, the hypermethylation of the TSG *HACE1* gene promoter was also observed
298 upon co-culture with *P. micra* phylotype A. *HACE1* is an E3 ubiquitin ligase controlling RAC1 stability, a
299 small GTPase of the Ras superfamily involved in cell motility (Torrino et al., 2011) and the TSG *HACE1*'s
300 promoter was previously shown to be hypermethylated in CRC (Zhang et al., 2007) with a broad down-
301 regulated expression in about 50% of all primary human tumors (Hibi et al., 2008). Loss of *HACE1*
302 expression predisposes animals to DSS-induced colitis and AOM-induced colon carcinogenesis (Tortola
303 et al., 2016). Hence, phylotype A of *P. micra* may cause epigenetic modifications that prepare or enhance
304 cell transformation through cytoskeleton rearrangement.

305 In conclusion, here we described the *P. micra* phylotype A as the most prevalent CRC-associated
306 Parvimonas, characterized by haemolytic capacity and adherent properties. Bacterial haemolysins have
307 been shown to cause epigenetic marks in histones (Hamon et al., 2007) but studies on DNA methylation
308 changes are lacking.

309 Clearly, further investigations on cross-talks between pathobionts, including *P. micra*, and the human
310 colonic epithelium are warranted. The next step will be to identify bacterial effectors that trigger adhesion
311 and directly or indirectly mediate epigenetic alterations in host cells.

312

313 **Acknowledgments**

314 The authors thank patients for having contributed to the present research program. We thank the
315 bacteriology Departments of Cochin, Pitié Salpêtrière, and Mondor Hospitals from APHP for providing *P.*
316 *micra* clinical isolates (particularly Drs Asmaa Tazi, Alexandra Aubry and Biba Nebbad) and the Collection
317 of Institut Pasteur for providing reference strains. We thank Claude Parsot and Shaynoor Dramsi for their
318 dedication and inspiration in the development of this work, and Pamela Schnupf for careful reading of the
319 manuscript. We acknowledge the URC of Henri Mondor and of St Antoine hospitals at APHP, Center for
320 Translational Science (CRT)-Cytometry and Biomarkers Unit of Technology and Service (CB UTechS) at
321 Institut Pasteur for their supports. This study was performed with the financial support from the Université
322 Paris Est Creteil (UPEC), PHRC (Vatnimad) of the French government, SNFGE (French society of

323 Gastroenterology Commad Support 2019), and from ITMO Cancer AVIESAN (Alliance Nationale pour
324 les Sciences de la Vie et de la Santé, National Alliance for Life Sciences & Health) within the framework
325 of the Cancer Plan (HTE201601) with the coordination of Mathias Chamailard, who was supported by
326 INCA, and executed within the frame of the Oncomix research program between Institut Pasteur and AP-
327 HP.

328

329 **Authors contributions**

330 Clinical and translational concept IS; basic conceptualization of *in vitro* study PS, GN, and EB;
331 methodology GN, EB, CP, SD, EL; investigation FD, TP, CP, GN and EB; formal analysis AD, DM, SV,
332 GN and EB; writing – original draft GN and EB; writing – review & editing GN, PS and IS; funding
333 acquisition and resources EL, PS, and IS; and supervision PS, IS and GN.

334 **Declaration of interests**

335 The authors declare no competing interests regarding these data and materials.

336 **Figures Legends**

337 **Figure 1: *P. micra* exists in two phylotypes with phenotypic and genetic diversity.**

338 A) Phylogenetic tree based on full length 16S rDNA sequences of 27 *P. micra* clinical isolates (named
339 *PMX*) and 22 reference sequences from the NCBI database. Root: *Finegoldia magna* ATCC 29328. The
340 infection type from which the 27 clinical isolates are derived are indicated by a color code; haemolysis
341 and colony compaction abilities are indicated as present (Y) or absent (N). B) Adhesion capacity of *P.*
342 *micra* ATCC 33270 (*PmA*) and HHM BINA17 (*PmB*) to extracellular matrix proteins. Optical density at
343 595 nm represents measurement of bacterial adhesion. C) Adhesion capacity of *PmA* and *PmB* to
344 different human colonic cell lines (TC7, HT-29, and HCT116) after 1 hour of co-culture. Bacterial adhesion
345 was quantified by the analysis of fluorescent images of cells co-cultured with the two phylotypes and is
346 reported as arbitrary fluorescent units (x100). Data are represented as mean \pm SEM from three
347 independent experiments. Mann-Whitney test ** $p < 0.01$; * $p < 0.05$. D). Positive contrast transmission
348 electron microscopy on ultrafine sections of *PmA* (top) and *PmB* (bottom). Spiky surface structures
349 (arrow) were observed only in *PmB* and not in *PmA*. Scale: 200 nm. See also Figure S1 and Table S1.

350

351 **Figure 2: *P. micra* phylotype A is associated with CRC.**

352 *Parvimonas* abundance, determined by 16S rDNA sequencing of the V3-V4 region, in controls, adenoma
353 (Ad.), or sporadic CRC patients at early (CRC I & II) and late (CRC III & IV) stages of carcinogenesis in
354 A) feces (Test Mann-Whitney *** $p < 0.001$; ** $p < 0.01$) or B) mucosa: on the left, normal homologous
355 mucosa versus tumoral tissue of CRC patients (Wilcoxon's Signed Wilcoxon Rank Test for paired
356 samples ** $p < 0.01$); on the right, the same results only in tumoral tissue and according to CRC stages
357 development. C) *P. micra* A and B phylotypes abundance in control and CRC patients' feces, or D)
358 associated with normal homologous mucosa and tumoral tissue of CRC patients. *P. micra* phylotypes
359 association with CMI (cumulative methylation index) methylation score of the WIF1, PENK, and NPY
360 genes promoters in E) controls and sporadic CRC patients' feces, or F) associated with tumoral tissue of
361 CRC patients. Results are expressed as a percentage of count (number of sequences assigned to
362 *Parvimonas* per number of total bacterial sequences X100) mean \pm SEM. Statistical analysis of C, D,
363 E, and F using the Mann-Whitney test ** $p < 0.01$, * $p < 0.05$. See Table S2.

364

365 **Figure 3: *P. micra* impact on human colonic primary epithelial cells.** A) Colonic organoids obtained
366 from normal tissue of CRC patients and cultured in Matrigel® with growth factors-enriched medium. B)
367 Schematic representation of Transwell® permeable insert used to cultivate monolayers of primary colonic
368 epithelial cells derived from organoids. C) Representative phase contrast images of organoid monolayers
369 at seeding (d-5), after 3 days of culture in aerobic conditions (d-2) and after 7 days of culture, including 4
370 days in aerobic conditions and 3 days in hypoxic conditions (d2). D) Transepithelial electrical resistance
371 (TEER) at different days of culture. TEER experiments were performed on cells from two donors, for at
372 least 4 experiments per donor. Results are expressed as a mean of Ohm per cm² +/- SEM. Mann-Whitney
373 test **p<0.01. E) The differentiation of the monolayers after 4 days in aerobic conditions and 3 days in
374 hypoxic conditions (2% O₂) was assessed by confocal microscopy. Nuclei (DAPI) are shown in grey, actin
375 (phalloidin) in red, microvilli (anti-villin) in yellow, tight junctions (anti-occludin) in dark blue, Colonocytes
376 (anti-KRT20) in cyan, Goblet cells (anti-muc2) in green, and enteroendocrine cells (anti-ChrA) in
377 magenta. Main panels, XY projection; right panels, YZ projection; bottom panels, XZ projection. F) Co-
378 culture experimental design with *P. micra* ATCC 33270 (*PmA*), HHM B1Na17 (*PmB*), and *F. magna*. G)
379 Cell viability after 48 hours of co-culture under hypoxic conditions at 37°C in 5% CO₂. Living cells were
380 quantified by flow cytometry and presented as the ratio of living cells in stimulated versus non-stimulated
381 samples (NS). H) Quantification of NF-κB positive nuclei upon immunofluorescent labeling with an anti-
382 p65 antibody and nuclear staining. Results are expressed as ratios of p65-positive nuclei over the total
383 number of nuclei and normalized by the NS condition. In G and H, results are from cells derived from two
384 donors with at least 3 independent experiments per donor and the data are represented as mean +/-
385 SEM. Mann-Whitney test ***p<0.001, **p<0.01, *p<0.05. See also Figure S2.

386

387 **Figure 4. *P. micra* phylotype A induces DNA methylation changes.** A) Global DNA methylation
388 dosage by quantification of 5-methyl-cytosine (5m-C) residues compared to total cytosines, after 48 hours
389 of co-culture of bacteria with human colonics monolayers. Results are expressed as the percentages of
390 5-mC normalized to the non-stimulated samples (NS). Experiments were performed on cells from two
391 donors, with at least 3 experiments per donor and data are represented as mean +/- SEM. Mann-Whitney
392 test *p<0.05. B and C) Gene number and distribution of hypo- and hyper-methylated genes between *P.*

393 *micra* ATCC 33270 (*PmA*), *P. micra* HHM BINA17 (*PmB*) phylotypes, or *F. magna* ATCC 29328 and the
394 NS condition. Differentially methylated genes were obtained by calculating a combined p-value based on
395 differentially methylated CpG sites located at specific genomic regions (TSS, in gene promoters; or non-
396 TSS, not at promoter sites) and regions within CpG islands or not. D) Venn diagram of differentially
397 methylated genes when only promoters (TSS) and CpG islands were considered. E) Heat map of fold-
398 change of the top 15 most differentially methylated genes (hypo- and hyper-methylated) in the
399 comparison of each bacterium- versus non-stimulated condition. CpG sites only in promoters (TSS) and
400 in CpG islands were considered. Whether these genes belonged to oncogenes, tumor suppressor genes
401 (TSGs) or epithelial-mesenchymal transition (EMT) databases, is indicated by a cross. See also Table
402 S3.

403

404 **Figure S1: Phenotypic and genetic characterization of *P. micra*.** A) Colony appearance of ATCC
405 33270 (*PmA*) (top) and HHM BINA17 (*PmB*) (bottom) on blood agar plates: i) after 48 hours of culture
406 under anaerobic conditions at 37°C; ii) when the colonies were removed to observe the haemolytic zone
407 below the colonies; and iii) when colonies were analyzed via the Gram stain. B) Sedimentation assay
408 performed on *PmA* and *PmB*. On the right, representative pictures of the suspension (top *PmA*, bottom
409 *PmB*) obtained after 2 hours at 4°C without shaking. C) Clustering of *P. micra* phylotype A and B whole
410 genomes according to the presence (red) or absence (blue) of genes.

411

412 **Figure S2:** A) *P. micra* oxygen sensitivity. Representative growth curves of *P. micra* ATCC 33270 (*PmA*)
413 under anaerobic (0% O₂), aerobic (21% O₂) and hypoxic (2% O₂) conditions. At different incubation times,
414 the cultures were plated on horse blood plates and returned to anaerobic conditions for 48 hours. CFUs
415 were counted to estimate bacterial viability. The results are expressed as percentage of CFU obtained
416 towards the inoculum grown at 0% O₂. B) *P. micra* viability by CFU counts after 48 hours of co-culture
417 with human colonic primary cells in hypoxic conditions (mean +/- SEM). C, D, and E. Quantification of
418 proliferative cells, cells harboring double-stranded DNA breaks, and goblet cells by immunofluorescence
419 using respectively an anti-Ki67, anti-γH2ax, and anti-Muc2 labelling after 48 hours of co-culture with *P.*
420 *micra* ATCC 33270 (*PmA*), *P. micra* HHM BINA17 (*PmB*), *F. magna* ATCC 29328 or the *E. coli* *Pks+*
421 strain IHE3034 (used as a positive control for double-stranded breaks). NS, non-stimulated. Results are

422 expressed as percentages of positive cells relative to the total number of nuclei and normalized using the
423 non-treated sample (NS). Experiments were performed on cells from two donors, with at least 3
424 experiments per donor. The data are represented as mean +/- SEM. Mann-Whitney test *** $p < 0.001$. F,
425 G, and H are representative images of Ki67, γ H2ax, and Muc2 immunostaining, respectively.

426

427 **Table S1:** Description of *P. micra* clinical isolates obtained from several hospitals in Paris and from
428 different infectious locations.

429

430 **Table S2:** Clinical data.

431

432 **Table S3: *PmA* induces DNA methylation changes in promoters of genes involved in**
433 **carcinogenesis.** CRC: colorectal cancer; TSG: tumor suppressor gene; EMT: epithelial-mesenchymal
434 transition; IGFs: insulin-like growth factors; SCF: SKP1-CUL1-F-box protein; TRAPP: transport protein
435 particle; ESCC: esophageal squamous cell carcinoma.

436 **Materials and Methods**

437 **Patient recruitment at the Créteil Henri Mondor Hospital**

438 Participants were selected from different cohorts recruited with informed consent between 2004 and 2018
439 by the endoscopy department at Henri Mondor hospital (Créteil) where patients had been referred for
440 colonoscopy; detailed description in (Sobhani et al., 2011). Participants with previous colon or rectal
441 surgery, colorectal cancer, inflammatory bowel diseases, or with a genetic form of CRC were excluded.
442 Individuals exposed to antibiotics or probiotics within four weeks before collection or suffering from acute
443 diarrhea were also excluded from the study. Tumor Node Metastasis (TNM) stages of colonic neoplasia
444 were determined by radiological examinations and analyses of the surgical specimen by the
445 anatomopathological department of Henri Mondor Hospital. Clinical parameters of the patients, such as
446 body mass index (BMI), age, sex, and disease history were referenced. The cumulative methylation index
447 (CMI) score was previously determined (Sobhani et al., 2011). This score was calculated from the
448 methylation status of three genes (*wif1*, *penk* and *npv*) involved in colorectal carcinogenesis and was
449 considered negative for $CMI < 2$ or positive for $CMI \geq 2$. Clinical data are summarized in Table S2.

450 **Fecal and tissue samples**

451 Fresh feces were collected between 2 weeks and 3 days prior to colonoscopy and ten grams were frozen
452 at -20°C for 4 hours and then stored at -80°C until use. Paired samples of colorectal tumor tissue and
453 homologous normal mucosa (more than 15 cm from the margin of tumor resection) were collected within
454 30 minutes after surgical resection and immediately frozen in liquid nitrogen and stored at -80°C until
455 further use.

456 **DNA extraction and quantification**

457 DNA extraction from fecal samples was performed using the G'NOME DNA isolation kit® (MP
458 Biomedicals) according to the supplier's instructions, with modifications as described in (Furet et al.,
459 2009). DNA extraction from tissue samples was performed from eight 50 μm cryosections of nitrogen
460 frozen tissue using the QIAamp PowerFecal DNA Kit® (Qiagen) following the supplier's instructions with
461 an additional lysis step (0.1 mm diameter silica beads were added to the lysis solution provided and
462 shaking was performed at maximum speed for 10 minutes in a vibratory shaker). Fecal and tissue DNA
463 concentrations were determined by Qubit® fluorometer (ThermoFisher) and stored at -20°C until use.

464 **Whole genome sequencing (WGS) of fecal samples**

465 Metagenome sequencing was performed by the high-throughput platforms BIOMICS (Institut Pasteur,
466 Paris, France) and EMBL (Heidelberg, Germany). Sequencing was performed in pairs, using the HiSeq
467 2000/platform 2500 equipment, over a length of 100 bp of DNA and at a sequencing depth of 5 Gbp
468 (Zeller et al., 2014). The raw data have already been reported in several papers (Schmidt et al., 2019;
469 Sobhani et al., 2011; Zeller et al., 2014). For this study, one hundred and sixty-six fecal samples from the
470 CCR1 and DETECT cohorts were considered. The Diamond/MEGAN6 bioinformatics pipeline (Bağcı et
471 al., 2019) was used for metagenomic assignment. Sequences were filtered for an average quality (Phred
472 score) greater than 20 over a window of two consecutive bases and a length greater than 100 bp using
473 Trimmomatic software (version 0.35). Good quality sequences were translated in the six possible reading
474 frames and aligned to the NR reference library (RefSEQ non-redundant protein database) in which
475 proteins/peptides that are more than 99% similar are combined into a single organism-associated group
476 with a specific identifier (O'Leary et al., 2016). A sequence can be assigned to several taxa. The MEGAN6
477 LCA (Lowest Common Ancestor) algorithm (Huson et al., 2016) was used to resolve multi-mapping reads:
478 when a sequence was assigned to two (or more) taxa of different phylogeny, it was assigned to the top
479 taxonomic level in common.

480 **16S rDNA sequencing of tissue samples**

481 For this study, 71 pairs of homologous tissue samples (matched tumor and healthy tissue) were analyzed.
482 After amplification of the 16S rRNA gene V3-V4 region, pairwise sequencing was performed to a length
483 of 250 bp on the Illumina MiSeq platform. The resulting raw database was cleaned of sequences
484 corresponding to human or phage sequences. Adapters and primers, as well as 5' and 3' ends with a
485 Phred quality score over a 2 bp sliding window of less than 30 were removed using Trimmomatic (version
486 0.35) software. Paired sequences were merged using the FLASH2 tool (version 2.2.00). Taxonomic
487 assignments were performed using MALT/MEGAN6 bioinformatic pipeline (Huson et al., 2016) with
488 default parameters and the SILVA rRNA database version 123 (Quast et al., 2012). OTUs were clustered
489 at a threshold of 97% identity.

490 **Colonic cell cultures**

491 Cancer cell lines: human colon cell lines HT-29, HCT116 and Caco-2 (subclone TC7), were grown in
492 DMEM ("Dulbecco Modified Eagle Medium") 1 g/L glucose (Gibco), supplemented with 20% (vol/vol)

493 decomplexed fetal bovine serum (FBS) (Gibco), 1% non-essential amino acids (Gibco), 1%
494 GlutaMAX (Gibco), at 37°C in 10% CO₂.

495 **Human colonic organoids**

496 Human colonic surgical resection specimens were obtained from Henri Mondor Hospital from two patients
497 who had undergone colectomy surgery from rectal adenocarcinoma and had given their informed consent
498 (agreement N°2012-37). Tissues samples from the normal site (far from tumor tissue) were sterilely
499 washed using PBS supplemented with gentamicin (50 µg/mL), Normoxin (1 mg/mL) and amphotericin B
500 (2 µg/mL), to obtain bacteria-free normal colonic mucosa and kept in 0.1% PBS-BSA at 4°C for the
501 duration of transport (approximately 4 hours). Crypts were isolated according to the protocol of Sato et
502 al, (Sato et al., 2011), with some modifications. The epithelium was stripped of underlying muscularis and
503 serosa, washed several times in cold PBS until the supernatant was clear, and cut into 5 mm² fragments.
504 The fragments were incubated for 20 minutes on ice in cold chelation buffer consisting of 5.6 mmol/L
505 Na₂HPO₄, 8.0 mmol/L KH₂PO₄, 96 mmol/L NaCl, 1.6 mmol/L KCl, 44 mmol/L sucrose, 54.8 mmol/L D-
506 sorbitol, and 0.5 mmol/L DL-dithiothreitol in distilled water plus 2 mmol/L EDTA. After removal of the
507 supernatant and addition of cold chelation buffer without EDTA, the tissue fragments were vigorously
508 resuspended by several passes through a 10 mL serological pipette. After sedimentation of the tissue
509 fragments, the supernatant, containing the crypts, was recovered. The resuspension/sedimentation
510 procedure was repeated twice. The tissue fragments were again incubated in chelation buffer with EDTA
511 for 15 minutes and the resuspension/sedimentation procedure was repeated three times. Fractions
512 containing crypts were pooled and centrifuged at 300g for 5 minutes. The crypt pellet was resuspended
513 in Matrigel® growth factor-reduced medium (Corning) diluted to 75% in culture medium (see composition
514 below). Four 25 µl drops of the Matrigel-crypt mixture were placed per well in 12-well plates with
515 approximately 100 crypts per drop. The plates were incubated for 15 minutes at 37°C to allow
516 polymerization of the Matrigel, then 800 µL of culture medium was added and the plates were incubated
517 at 37°C and 5% CO₂. The culture medium consisted of AdvancedDMEM/F12 (Gibco), 10 mM HEPES
518 (Gibco), 1X GlutaMAX (Gibco), 100 U/mL penicillin, 100 µg/mL streptomycin (Gibco), 1X N2
519 (ThermoFisher), 1X B27 (ThermoFisher), 1 mM N-acetyl-L-cysteine (Sigma), 100 ng/mL Noggin (R&D
520 systems), 50 ng/mL recombinant human EGF (R&D systems), 150 ng/mL Wnt-3A (R&D systems), 1
521 µg/mL recombinant human R-spondin-1 (R&D systems), 500 nM A83-01 (R&D systems), 10 mM

522 nicotinamide (Sigma), 10 μ M SB202190 (Sigma), 10 nM Gastrin I (Sigma), 3 μ M CHIR99021 (Biogems),
523 10 μ M Y27632 (Sigma) and 10% decompemented fetal bovine serum (vol/vol) (Gibco). The culture
524 medium was changed every two days, without Y27632. Each week, organoids were split with a 1:3 ratio.
525 The medium was replaced by cold fresh medium and the Matrigel drops and the organoids were
526 dissociated by pipetting several times through a 200 μ l tip and collect in a tube. After a spin for 5 minutes
527 at 300g at 4°C, the pellet was washed with fresh cold medium, resuspended with a p200 pipette several
528 times, and spun again. The pellet of organoid fragments was resuspended and diluted in Matrigel® as
529 described above. After expansion, organoids were frozen and stored at -80°C in freezing medium
530 composed of AdvancedDMEM/F12, 10% fetal bovine serum, 10% DMSO (PAN Biotech), 10 μ M Y-27632
531 and 3 μ M CHIR99021.

532 **Generation of human colonic epithelial monolayer**

533 Monolayers of organoid-derived primary cells were generated as previously described (Noel et al., 2017).
534 Briefly, the twenty-four well plates with 0.4 μ m pores (Corning) Transwell® insert system were used as
535 culture support for primary cells in monolayers. Inserts were previously coated with 50 μ l of human
536 collagen IV at 30 μ g/ml (Millipore) overnight at 4°C, then washed with DMEM. Approximately three
537 hundred organoids at five days of growth were dissociated into fragments (using Cell Recovery
538 (Corning)), resuspended in 200 μ l of culture medium and put on each insert. The culture medium
539 consisted of DMEM/F12 (Gibco), 10 mM HEPES (Gibco), 1X GlutaMAX (Gibco), 100 u/mL penicillin, 100
540 μ g/mL streptomycin (Gibco), 1X N2 (ThermoFisher) and B27 (ThermoFisher) supplements, 1 mM N-
541 acetyl-L-cysteine (Sigma), 100 ng/mL noggin (R&D systems), 50 ng/mL recombinant human EGF (R&D
542 systems), 150 ng/mL Wnt-3A (R&D systems), 1 μ g/mL recombinant human R-spondin-1 (R&D systems),
543 500 nM A83-01 (R&D systems), 10 mM nicotinamide (Sigma), 10 μ M SB202190 (Sigma), 10 nM Gastrin
544 I (Sigma), 3 μ M CHIR99021 (Biogems), 10 μ M Y27632 (Sigma) and 10% decompemented fetal bovine
545 serum (vol/vol) (Gibco). Monolayers were incubated at 37°C in 5% CO₂. After three days of culture, the
546 medium was changed without addition of Y-27632. Cell growth and monolayer closure were monitored
547 daily by observation with an inverted brightfield microscope (IX81, Olympus) and by recording the
548 transepithelial electrical resistance (Millipore).

549 **Bacterial strains, culture and characterization**

550 *Escherichia coli* pks+ strain IHE3034 was used as a positive control for double-strand DNA breaks.
551 *Shigella flexneri* 5a BS176, lacking the virulence plasmid, was used as a negative control for bacterial
552 adhesion and autoaggregation negative control. The reference strains ATCC 33270 of *P. micra* (*PmA*)
553 and ATCC 29328 of *Fingoldia magna* were obtained from the Pasteur Institute Collection (CIP). In this
554 study, twenty-seven clinical isolates of *P. micra*, including HHM B1Na17 (*PmB*), were collected from the
555 bacteriology departments of three Parisian hospitals: Henri Mondor, Cochin, and Pitié Salpêtrière (Table
556 S1). The identification of the different isolates was confirmed by mass spectrometry and 16S rDNA
557 sequencing analysis (Eurofins Genomics) and sequences were deposited on GenBank (Table S1). 16S
558 rDNA whole sequence from positions 112 to 1302 were aligned with the ClustalW program (EMBL) and
559 the phylogenetic tree was calculated using the PhyML program. Pan-genomic comparison: available
560 complete *P. micra* genomes were downloaded from the NCBI database. Analysis of pangenomes and
561 comparison of common or strain-specific gene carriage was performed using the Roary program (Page
562 et al., 2015) with a 95% identity threshold and the use of default parameters.

563 **Culture:**

564 Bacteria were grown under anaerobic conditions in TGY-V enriched broth (Trypticase peptone 30 g/L, D-
565 glucose 10 g/L, Yeast extract 20 g/L, L-cysteine-HCl 0.5 g/L, haemin 5 mg/L, vitamin B12 5 µg/L,
566 menadione sodium bisulfite 500 µg/L, Thiamine 1 mg/L, nicotinic acid 1 mg/L, riboflavin 500 µg/L, p-
567 aminobenzoic acid 100 µg/L, biotin 25 mg/L, calcium pantothenate 1 mg/L, pyridoxamine 2HCl 500 µg/L,
568 folic acid 500 µg/L) or on Columbia agar solid support enriched with 5% horse blood (COH) (Biorad).
569 Anoxic conditions were generated in Gaspack (BD) or anaerobic cabinet (Don Whitley DG250
570 Workstation). Hemolysis ability and colonies compactions were assessed by observing CFUs on COH
571 plates after 48 hours at 37°C in anaerobic conditions: i) contact haemolytic activity was defined by the
572 presence of an haemolytic zone located underneath the colony and slightly beyond (Figure S1A) and ii)
573 colonies compaction was defined as “non-compact” or “compact”: the “non-compact” colonies spread out
574 on agar upon contact with a loop, whereas the compact colonies remained associated in clumps
575 suggesting a strong interbacterial aggregative property. For the sedimentation assay, bacteria were
576 grown on blood agar plates under anaerobic conditions at 37°C for 48 hours, resuspended in PBS, and
577 incubated at 4°C statically. The optical density (600 nm) in the upper half of the test tubes was measured
578 periodically (Figure S1B).

579 **Transmission electron microscopy:**

580 Bacteria from a 4 day-old cultures were fixed by adding glutaraldehyde (2.5% final concentration) to the
581 culture for 1 hour at room temperature (RT). The bacteria were washed twice with HEPES 0.1 M, pH 7.5
582 and postfixed with 1% osmium tetroxide in HEPES 0.1 M pH 7.5 for 1h30 at RT. After three washes in
583 distilled water, the bacteria were dehydrated in a graded ethanol series (25, 50, 75, 95 and 100% ethanol),
584 and gradually infiltrated in Epon resin. Ultrathin sections (60 nm) were obtained on a FC6/UC6
585 ultramicrotome (Leica). Sections were transferred to 200 Mesh Square Copper grids (CF-200-CuO, Delta
586 Microscopy) formvar and carbon coated, stained with 4% uranyl acetate, and counterstained with
587 Reynold's lead citrate for 20 minutes. Images were recorded with TECNAI SPIRIT 120 Kv, with a bottom-
588 mounted EAGLE 4KX4K Camera.

589 **Bacteria adhesion**

590 Adhesion to extracellular matrix proteins: MaxiSorp 96-well flat-bottom plates (ThermoFisher) were
591 coated overnight at 4°C under agitation with 1 µg per well, in triplicate, with the following extracellular
592 matrix proteins: collagen I (Gibco), collagen IV (Millipore), fibronectin (Gibco), fibrinogen (Sigma), laminin
593 (Sigma), and Matrigel® (consisting of a mixture of proteins, mainly laminin, collagen IV, entactin, and
594 heparan sulfate proteoglycan) (Corning). Bacteria were grown on COH plates for 48 hours at 37°C under
595 anaerobic conditions, collected and suspended in PBS at an OD of three units. The bacterial suspension
596 was placed in the wells and the plate was centrifuged at 300g for 5 minutes. After incubation for 1 hour
597 at RT, the wells were washed three times with PBS to remove non-adherent bacteria and then stained
598 with 0.1% crystal violet (Sigma). The plates were incubated for 30 minutes at RT and washed three more
599 times with PBS. The dye was dissolved with 20:80 acetone-ethanol and the optical density at 595 nm
600 was read by a spectrometer (Infinite M200Pro-TECAN).

601 *P. micra* adhesion to colonic cell lines: human colonic cell lines (TC7, HT-29, and HCT116) were grown
602 on glass coverslips in 24-well plates to confluence. In parallel, *P. micra* was grown on COH plates for 48
603 hours at 37°C under anaerobic conditions. Bacteria were washed in PBS, re-suspended in DMEM with 1
604 g/L glucose (Gibco), and put on the cells using a M.O.I. of 1. The plates were centrifuged for 5 minutes
605 at 300g and incubated for 1 hour at 37°C. After incubation, the cells were washed three times in PBS,
606 fixed in 4% paraformaldehyde (PFA) (Electron Microscopy Sciences) for 30 minutes at RT, washed again
607 three times in PBS, and then stored in 0.1% PBS-BSA at 4°C until labeling. Non-specific sites were

608 blocked with 1% PBS-BSA for 1 hour at RT. The cells were then incubated with rabbit anti-*Parvimonas*
609 serum (on order by Covalab) at 1:1000 in 1% PBS-BSA for 30 minutes at room temperature. After
610 washing, the cells were permeabilized with PBS- 0.2% triton for 30 minutes. Anti-rabbit secondary
611 antibody coupled to Alexa Fluor 488 (ThermoFisher) at 1:400 and phalloidin coupled to Alexa Fluor 568
612 (Invitrogen) at 1:200 were used in 1% PBS-BSA for 45 minutes at RT. After washing, nucleic acids were
613 labeled with 1 µg/mL DAPI (ThermoFisher) for 5 minutes. The coverslip with the cells were washed again
614 and mounted on a slide with Prolong Gold (ThermoFisher). Images were taken using a slide scanner with
615 40X objective (AxioScan, Zeiss) and processed using Fiji (Schindelin et al., 2012). Bacterial adhesion
616 was quantified as area of the anti-*Parvimonas* fluorescence signal over an entire field normalized by the
617 total number of nuclei and reported as arbitrary fluorescent units x100.

618 **Co-culture of colonic cells and *P. micra***

619 Bacteria were grown in TGY-V medium under anaerobic conditions at 37°C for 48 hours, followed by a
620 1:10 subculture for 24 hours to reach exponential phase. Bacterial density was adjusted to an M.O.I. of
621 250 in cell culture medium and then put on the cells. Twenty-four hours prior to bacterial exposure, the
622 colonic cells were placed in 2% O₂ in H35 hypoxic cabinet (Don Whitley) to allow acclimatization. Co-
623 cultures with primary cells were performed for 48 hours at 37°C under hypoxic conditions.

624 **Flow cytometry**

625 Cell monolayers were dissociated with TrypLE™ Express Enzyme (Gibco) at 37°C for ten to twenty
626 minutes. The cells were recovered in DMEM/F12 at RT and then centrifuged for five minutes at 300g.
627 After washing the pellet in PBS, cells were stained with the Live/Dead fixable cell stain kit (ThermoFisher)
628 for twenty minutes on ice, following the supplier's instructions. Cells were analyzed using a FACS Attune
629 (ThermoFisher) and data were analyzed using FlowJo software (v10.1).

630 **Ki-67, γH2ax, Muc2 and NF-κB immunofluorescence**

631 Following 48 hours co-culture with *P. micra*, cells were washed with PBS, fixed (4% PFA, 30 minutes),
632 washed again, and stored (0.1% PBS-BSA) at 4°C until labeling. Cells were permeabilized with 0.5%
633 Triton-PBS for 30 minutes at RT, washed in 0.1% PBS-Triton, and blocked with 1% bovine serum albumin
634 (BSA)-0.1% Triton for 30 minutes. The cells were then incubated either i) with a 1:200 dilution of an
635 antibody against the proliferation marker Ki-67 coupled to Alexa Fluor 666 (clone SolA15, eBioscience)
636 and a 1:500 dilution of an antibody against the phosphorylated form of H2A histone family member X

637 (γ H2Ax) (clone JBW301, Merck) and 1:200 phalloidin coupled to Alexa Fluor 568; ii) a 1:50 dilution of an
638 antibody against nuclear factor kappa-light-chain-enhancer of activated B cells (NF- κ B) p65 (ab7970
639 Abcam) and 1:200 phalloidin coupled to Alexa Fluor 568; or iii) with a 1:100 dilution of an anti-mucin2
640 (Muc2) antibody (clone Ccp58, Abcam) and 1:200 phalloidin coupled to Alexa Fluor 568, in 0.1% Triton-
641 BSA overnight at 4°C. After washing in 0.1% PBS-Triton, the cells were incubated with 1:400 secondary
642 antibodies coupled to Alexa Fluor 488 (ThermoFisher) in 0.1% PBS-Triton for 45 minutes at RT. Cells
643 were washed again in 0.1% PBS-Triton and the nucleic acids were labeled with 1 μ g/mL DAPI for 5
644 minutes before cells were mounted on a slide with ProlongGold (ThermoFisher). Fluorescence images
645 were taken using a confocal fluorescence microscope (Zeiss) equipped with an Opterra system (Bruker),
646 and the number of cells was analyzed as the number of positive cells/total cells using Fiji (Schindelin et
647 al., 2012) or Imaris 9.8 software (URL: <http://www.bitplane.com/Imaris/Imaris>) software.

648 **DNA methylation studies**

649 Human cells co-cultured with *P. micra* were subjected to DNA extraction using the DNeasy Blood &
650 Tissue Kit® (Qiagen) according to the manufacturer's instructions and DNA was quantified using a Qubit®
651 fluorometer.

652 Global DNA methylation level: MethylFlash methylated DNA Quantification Fluorometer Kit (Epigentek)
653 was used to detect the global methylation level in DNA isolated from primary colonic cells co-cultured
654 with *P. micra* ATCC 33270 (*PmA*), HHM BINA17 (*PmB*) and *F. magna*. Assays were performed in
655 duplicate. As instructed by the manufacturer, 100 ng of the isolated genomic DNA was bound to the assay
656 well. The capture antibody, detection antibody, and enhancer solution were then added consecutively to
657 the wells before the fluoro-developing solution was added and the relative fluorescence units (RFU) were
658 measured (TECAN). The percentage of 5-methylcytosine (5-mC) relative to the total amount of cytosines
659 in the sample was calculated to represent the global methylation dosage and was reported as a ratio to
660 the non-stimulated samples.

661 DNA methylation profiling: DNA methylation profiling was performed on eight independent co-cultures of
662 *PmA*, *PmB*, and *F. magna* with human primary colonic cells (four experiments per patient tissue). The
663 Infinium MethylationEPIC BeadChip Kit (850K) (Illumina, San Diego, CA, USA) was used for a genome-
664 wide methylation profiling to determine the DNA methylation status of >850,000 CpG sites (Moran et al.,
665 2016). A total of 500 ng of genomic DNA from cells in co-cultures were bisulfite-treated using the

666 ZymoResearch EZ DNA Methylation kit (Zymo Research Corp, Irvine, CA, USA). The Infinium HD
667 Methylation Assay (bisulfite modification, amplification, fragmentation, precipitation, hybridization, wash,
668 extension, staining, and imaging) was performed according to the manufacturer's explicit specifications.
669 The quality was supported by multiple quality control (QC) measures, including tests for proper bisulfite
670 conversion, staining, and specificity of the internal controls, as determined by Illumina GenomeStudio
671 software. Average-beta values (proxy for methylated DNA level between 0, unmethylated, and 1, fully
672 methylated) were normalized to internal controls and corrected by background subtraction. Non-
673 autosomal CpGs (n=14,522) and CpG probes with suboptimal detection ($p < 0.05$ in at 80% of samples)
674 (n= 29,316), as well as single nucleotide polymorphisms (SNPs) associated CpGs (n=59), were removed
675 from our analyses. Beta values were transformed into M-values as described by (Du et al., 2010), to be
676 able to use the Limma statistical model (Wettenhall and Smyth, 2004) package R Limma, version 4.0.2.
677 The four conditions (Non-stimulated NS; ATCC; BINa and FM) and individuals were kept as variables.
678 Pairwise comparisons were obtained from a contrast matrix. No adjustment method was used. For each
679 gene (n=25,560), a t-test on log-fold-change was performed on four categories of probes depending on
680 their CpG context and gene localization: probes in CpG island context and 1/ localized in genes promoters
681 (TSS1500+TSS200) or 2/ in body gene; and probes out of CpG island context 3/ in promoters or 4/ in
682 body gene. Genes with >2probes, p-value <0.05, and with a log-FC >0,1 (absolute value) were
683 considered significant. Using three different databases, the genes were classified as oncogenes, tumor
684 suppressor genes, or involved in Epithelial-Mesenchymal Transition (ONGene (Liu et al., 2017), TSGene
685 2.0 (Zhao et al., 2016) or dbEMT 2.0 (Zhao et al., 2019).
686

687 **References**

- 688 Bağcı, C., Beier, S., Górska, A., and Huson, D.H. (2019). Introduction to the analysis of environmental
689 sequences: Metagenomics with MEGAN. In *Methods in Molecular Biology*, (Humana Press Inc.), pp.
690 591–604.
- 691 Becht, E., De Reyniès, A., Giraldo, N.A., Pilati, C., Buttard, B., Lacroix, L., Selves, J., Sautès-Fridman,
692 C., Laurent-Puig, P., and Fridman, W.H. (2016). Immune and stromal classification of Colorectal cancer
693 is associated with molecular subtypes and relevant for precision immunotherapy. *Clin. Cancer Res.* 22,
694 4057–4066.
- 695 Bowler, P.G., and Davies, B.J. (1999a). The Microbiology of Acute and Chronic Wounds. *Wounds* 11,
696 72–78.
- 697 Bowler, P.G., and Davies, B.J. (1999b). The microbiology of infected and noninfected leg ulcers. *Int. J.*
698 *Dermatol.* 38, 573–578.
- 699 Chan, D.S.M., Lau, R., Aune, D., Vieira, R., Greenwood, D.C., Kampman, E., and Norat, T. (2011). Red
700 and processed meat and colorectal cancer incidence: Meta-analysis of prospective studies. *PLoS One*
701 6, e20456.
- 702 Dejea, C.M., and Sears, C.L. (2016). Do biofilms confer a pro-carcinogenic state? *Gut Microbes* 7, 54–
703 57.
- 704 Dejea, C.M., Wick, E.C., Hechenbleikner, E.M., White, J.R., Mark Welch, J.L., Rossettid, B.J., Peterson,
705 S.N., Snesrud, E.C., Borisy, G.G., Lazarev, M., et al. (2014). Microbiota organization is a distinct feature
706 of proximal colorectal cancers. *Proc. Natl. Acad. Sci. U. S. A.* 111, 18321–18326.
- 707 Deplancke, B., and Gaskins, H.R. (2001). Microbial modulation of innate defense: Goblet cells and the
708 intestinal mucus layer. *Am. J. Clin. Nutr.* 73, 1131S-1141S.
- 709 Drewes, J.L., White, J.R., Dejea, C.M., Fathi, P., Iyadorai, T., Vadivelu, J., Roslani, A.C., Wick, E.C.,
710 Mongodin, E.F., Loke, M.F., et al. (2017). High-resolution bacterial 16S rRNA gene profile meta-analysis
711 and biofilm status reveal common colorectal cancer consortia. *Npj Biofilms Microbiomes* 3.
- 712 Du, P., Zhang, X., Huang, C.C., Jafari, N., Kibbe, W.A., Hou, L., and Lin, S.M. (2010). Comparison of
713 Beta-value and M-value methods for quantifying methylation levels by microarray analysis. *BMC*
714 *Bioinformatics* 11, 1–9.
- 715 Edmiston, C.E., Walker, A.P., Krepel, C.J., and Gohr, C. (1990). The nonpuerperal breast infection:
716 Aerobic and anaerobic microbial recovery from acute and chronic disease. *J. Infect. Dis.* 162, 695–699.
- 717 Fearon, E.R., and Vogelstein, B. (1990). A genetic model for colorectal tumorigenesis. *Cell* 61, 759–767.
- 718 Flemer, B., Lynch, D.B., Brown, J.M.R., Jeffery, I.B., Ryan, F.J., Claesson, M.J., O’Riordain, M.,
719 Shanahan, F., and O’Toole, P.W. (2017). Tumour-associated and non-tumour-associated microbiota in
720 colorectal cancer. *Gut* 66, 633–643.
- 721 Furet, J.P., Firmesse, O., Gourmelon, M., Bridonneau, C., Tap, J., Mondot, S., Doré, J., and Corthier, G.
722 (2009). Comparative assessment of human and farm animal faecal microbiota using real-time quantitative
723 PCR. *FEMS Microbiol. Ecol.* 68, 351–362.
- 724 Gao, R., Kong, C., Huang, L., Li, H., Qu, X., Liu, Z., Lan, P., Wang, J., and Qin, H. (2017). Mucosa-
725 associated microbiota signature in colorectal cancer. *Eur. J. Clin. Microbiol. Infect. Dis.* 36, 2073–2083.
- 726 Goodwin, A.C., Destefano Shields, C.E., Wu, S., Huso, D.L., Wu, X.Q., Murray-Stewart, T.R., Hacker-

- 727 Prietz, A., Rabizadeh, S., Woster, P.M., Sears, C.L., et al. (2011). Polyamine catabolism contributes to
728 enterotoxigenic *Bacteroides fragilis*-induced colon tumorigenesis. *Proc. Natl. Acad. Sci. U. S. A.* *108*,
729 15354–15359.
- 730 Guinney, J., Dienstmann, R., Wang, X., De Reyniès, A., Schlicker, A., Soneson, C., Marisa, L., Roepman,
731 P., Nyamundanda, G., Angelino, P., et al. (2015). The consensus molecular subtypes of colorectal
732 cancer. *Nat. Med.* *21*, 1350–1356.
- 733 Hamon, M.A., Batsché, E., Régnault, B., To, N.T., Seveau, S., Muchardt, C., and Cossart, P. (2007).
734 Histone modifications induced by a family of bacterial toxins. *Proc. Natl. Acad. Sci. U. S. A.* *104*, 13467–
735 13472.
- 736 Hibi, K., Mizukami, H., Shirahata, A., Goto, T., Sakata, M., Saito, M., Ishibashi, K., Kigawa, G., Nemoto,
737 H., and Sanada, Y. (2009). Aberrant methylation of the *UNC5C* gene is frequently detected in advanced
738 colorectal cancer. *Anticancer Res.* *29*, 271–273.
- 739 Horiuchi, A., Kokubu, E., Warita, T., and Ishihara, K. (2020). Synergistic biofilm formation by *Parvimonas*
740 *micra* and *Fusobacterium nucleatum*. *Anaerobe* *62*.
- 741 Huson, D.H., Beier, S., Flade, I., Górska, A., El-Hadidi, M., Mitra, S., Ruscheweyh, H.J., and Tappu, R.
742 (2016). MEGAN Community Edition - Interactive Exploration and Analysis of Large-Scale Microbiome
743 Sequencing Data. *PLoS Comput. Biol.* *12*, e1004957.
- 744 Jiao, S., Peters, U., Berndt, S., Brenner, H., Butterbach, K., Caan, B.J., Carlson, C.S., Chan, A.T., Chang-
745 Claude, J., Chanock, S., et al. (2014). Estimating the heritability of colorectal cancer. *Hum. Mol. Genet.*
746 *23*, 3898–3905.
- 747 Kamada, N., Chen, G.Y., Inohara, N., and Núñez, G. (2013). Control of pathogens and pathobionts by
748 the gut microbiota. *Nat. Immunol.* *14*, 685–690.
- 749 Koliarakis, I., Messaritakis, I., Nikolouzakis, T.K., Hamilos, G., Souglakos, J., and Tsioussis, J. (2019).
750 Oral bacteria and intestinal dysbiosis in colorectal cancer. *Int. J. Mol. Sci.* *20*, 4146.
- 751 Kremer, B.H.A., Magee, J.T., Van Dalen, P.J., and Van Steenberg, T.J.M. (1997). Characterization of
752 smooth and rough morphotypes of *Peptostreptococcus micros*. *Int. J. Syst. Bacteriol.* *47*, 363–368.
- 753 Kyrgiou, M., Kalliala, I., Markozannes, G., Gunter, M.J., Paraskeva, E., Gaba, H., Martin-Hirsch, P.,
754 and Tsilidis, K.K. (2017). Adiposity and cancer at major anatomical sites: Umbrella review of the literature.
755 *BMJ* *356*, 477.
- 756 Li, S., Konstantinov, S.R., Smits, R., and Peppelenbosch, M.P. (2017). Bacterial Biofilms in Colorectal
757 Cancer Initiation and Progression. *Trends Mol. Med.* *23*, 18–30.
- 758 Lin, Q., Li, J., Zhu, D., Niu, Z., Pan, X., Xu, P., Ji, M., Wei, Y., and Xu, J. (2019). Aberrant scinderin
759 expression correlates with liver metastasis and poor prognosis in colorectal cancer. *Front. Pharmacol.*
760 *10*, 1183.
- 761 Liu, Y., Sun, J., and Zhao, M. (2017). ONGene: A literature-based database for human oncogenes. *J.*
762 *Genet. Genomics* *44*, 119–121.
- 763 Lou, J., Huang, J., Dai, X.Y., Xie, Y., Dong, M.J., Chen, B., Zhao, J., Zhou, H., Zhou, B., and Yu, H.
764 (2017). Knockdown of tetraspanin 13 inhibits proliferation of colorectal cancer cells. *Int. J. Clin. Exp. Med.*
765 *10*, 6387–6395.
- 766 Martini, M., Gnann, A., Scheickl, D., Holzmann, B., and Janssen, K.P. (2011). The candidate tumor

767 suppressor SASH1 interacts with the actin cytoskeleton and stimulates cell-matrix adhesion. *Int. J.*
768 *Biochem. Cell Biol.* 43, 1630–1640.

769 Mazmanian, S.K., Cui, H.L., Tzianabos, A.O., and Kasper, D.L. (2005). An immunomodulatory molecule
770 of symbiotic bacteria directs maturation of the host immune system. *Cell* 122, 107–118.

771 Moran, S., Arribas, C., and Esteller, M. (2016). Validation of a DNA methylation microarray for 850,000
772 CpG sites of the human genome enriched in enhancer sequences. *Epigenomics* 8, 389–399.

773 Mousa, H.A.L. (1997). Aerobic, anaerobic and fungal burn wound infections. *J. Hosp. Infect.* 37, 317–
774 323.

775 Murdoch, D.A., Mitchelmore, I.J., and Tabaqchali, S. (1988). Peptostreptococcus Micros in Polymicrobial
776 Abscesses. *Lancet* 331, 594.

777 Noel, G., Baetz, N.W., Staab, J.F., Donowitz, M., Kovbasnjuk, O., Pasetti, M.F., and Zachos, N.C. (2017).
778 A primary human macrophage-enteroid co-culture model to investigate mucosal gut physiology and host-
779 pathogen interactions. *Sci. Rep.* 7.

780 Nougayrède, J.P., Homburg, S., Taieb, F., Boury, M., Brzuszkiewicz, E., Gottschalk, G., Buchrieser, C.,
781 Hacker, J., Dobrindt, U., and Oswald, E. (2006). Escherichia coli induces DNA double-strand breaks in
782 eukaryotic cells. *Science* 313, 848–851.

783 O’Leary, N.A., Wright, M.W., Brister, J.R., Ciufo, S., Haddad, D., McVeigh, R., Rajput, B., Robbertse, B.,
784 Smith-White, B., Ako-Adjei, D., et al. (2016). Reference sequence (RefSeq) database at NCBI: Current
785 status, taxonomic expansion, and functional annotation. *Nucleic Acids Res.* 44, D733–D745.

786 Page, A.J., Cummins, C.A., Hunt, M., Wong, V.K., Reuter, S., Holden, M.T.G., Fookes, M., Falush, D.,
787 Keane, J.A., and Parkhill, J. (2015). Roary: Rapid large-scale prokaryote pan genome analysis.
788 *Bioinformatics* 31, 3691–3693.

789 Pasquereau-Kotula, E., Martins, M., Aymeric, L., and Dramsi, S. (2018). Significance of Streptococcus
790 gallolyticus subsp. gallolyticus association with colorectal cancer. *Front. Microbiol.* 9, 614.

791 Pleguezuelos-Manzano, C., Puschhof, J., Rosendahl Huber, A., van Hoeck, A., Wood, H.M., Nomburg,
792 J., Gurjao, C., Manders, F., Dalmasso, G., Stege, P.B., et al. (2020). Mutational signature in colorectal
793 cancer caused by genotoxic pks + E. coli. *Nature* 580, 269–273.

794 Purcell, R. V., Visnovska, M., Biggs, P.J., Schmeier, S., and Frizelle, F.A. (2017). Distinct gut microbiome
795 patterns associate with consensus molecular subtypes of colorectal cancer. *Sci. Rep.* 7, 11590.

796 Quast, C., Pruesse, E., Yilmaz, P., Gerken, J., Schweer, T., Yarza, P., Peplies, J., and Glöckner, F.O.
797 (2013). The SILVA ribosomal RNA gene database project: Improved data processing and web-based
798 tools. *Nucleic Acids Res.* 41, D590–D596.

799 Rams, T.E., Feik, D., Listgarten, M.A., and Slots, J. (1992). Peptostreptococcus micros in human
800 periodontitis. *Oral Microbiol. Immunol.* 7, 1–6.

801 Rana, M.K., Aloisio, F.M., Choi, C., and Barber, D.L. (2018). Formin-dependent TGF- β signaling for
802 epithelial to mesenchymal transition. *Mol. Biol. Cell* 29, 1465–1475.

803 Rubinstein, M.R., Wang, X., Liu, W., Hao, Y., Cai, G., and Han, Y.W. (2013). Fusobacterium nucleatum
804 Promotes Colorectal Carcinogenesis by Modulating E-Cadherin/ β -Catenin Signaling via its FadA
805 Adhesin. *Cell Host Microbe* 14, 195–206.

806 Saffarian, A., Mulet, C., Regnault, B., Amiot, A., Tran-Van-Nhieu, J., Ravel, J., Sobhani, I., Sansonetti,

- 807 P.J., and Pédrón, T. (2019). Crypt- and mucosa-associated core microbiotas in humans and their
808 alteration in colon cancer patients. *MBio* 10, e01315-19.
- 809 Samad, A.K.A., Taylor, R.S., Marshall, T., and Chapman, M.A.S. (2005). A meta-analysis of the
810 association of physical activity with reduced risk of colorectal cancer. *Color. Dis.* 7, 204–213.
- 811 Sanderson, P.J., Wren, M.W.D., and Baldwin, A.W.F. (1979). Anaerobic organisms in postoperative
812 wounds. *J. Clin. Pathol.* 32, 143–147.
- 813 Schindelin, J., Arganda-Carreras, I., Frise, E., Kaynig, V., Longair, M., Pietzsch, T., Preibisch, S., Rueden,
814 C., Saalfeld, S., Schmid, B., et al. (2012). Fiji: An open-source platform for biological-image analysis. *Nat.*
815 *Methods* 9, 676–682.
- 816 Schmidt, T.S.B., Hayward, M.R., Coelho, L.P., Li, S.S., Costea, P.I., Voigt, A.Y., Wirbel, J., Maistrenko,
817 O.M., Alves, R.J.C., Bergsten, E., et al. (2019). Extensive transmission of microbes along the
818 gastrointestinal tract. *Elife* 8, e42693.
- 819 Schwabe, R.F., and Jobin, C. (2013). The microbiome and cancer. *Nat. Rev. Cancer* 13, 800–812.
- 820 Shimizu, A., Mammoto, A., Italiano, J.E., Pravda, E., Dudley, A.C., Ingber, D.E., and Klagsbrun, M.
821 (2008). ABL2/ARG tyrosine kinase mediates SEMA3F-induced RhoA inactivation and cytoskeleton
822 collapse in human glioma cells. *J. Biol. Chem.* 283, 27230–27238.
- 823 Sobhani, I., Tap, J., Roudot-Thoraval, F., Roperch, J.P., Letulle, S., Langella, P., Gérard, C., van Nhieu,
824 J.T., and Furet, J.P. (2011). Microbial dysbiosis in colorectal cancer (CRC) patients. *PLoS One* 6, e16393.
- 825 Sobhani, I., Bergsten, E., Couffin, S., Amiot, A., Nebbad, B., Barau, C., de'Angelis, N., Rabot, S., Canoui-
826 Poitrine, F., Mestivier, D., et al. (2019). Colorectal cancer-associated microbiota contributes to oncogenic
827 epigenetic signatures. *Proc. Natl. Acad. Sci. U. S. A.* 116, 24285–24295.
- 828 Socransky, S.S., Haffajee, A.D., Ximenez-Fyvie, L.A., Feres, M., and Mager, D. (1999). Ecological
829 considerations in the treatment of *Actinobacillus actinomycetemcomitans* and *Porphyromonas gingivalis*
830 periodontal infections. *Periodontol.* 2000 20, 341–362.
- 831 Soderholm, A.T., and Pedicord, V.A. (2019). Intestinal epithelial cells: at the interface of the microbiota
832 and mucosal immunity. *Immunology* 158, 267–280.
- 833 Torino, S., Visvikis, O., Doye, A., Boyer, L., Stefani, C., Munro, P., Bertoglio, J., Gacon, G., Mettouchi,
834 A., and Lemichez, E. (2011). The E3 ubiquitin-ligase HACE1 catalyzes the ubiquitylation of active Rac1.
835 *Dev. Cell* 21, 959–965.
- 836 Tortola, L., Nitsch, R., Bertrand, M.J.M., Kogler, M., Redouane, Y., Kozieradzki, I., Uribesalgo, I., Fennell,
837 L.M., Daugaard, M., Klug, H., et al. (2016). The Tumor Suppressor Hace1 Is a Critical Regulator of
838 TNFR1-Mediated Cell Fate. *Cell Rep.* 15, 1481–1492.
- 839 Wettenhall, J.M., and Smyth, G.K. (2004). limmaGUI: A graphical user interface for linear modeling of
840 microarray data. *Bioinformatics* 20, 3705–3706.
- 841 Xia, X., Wu, W.K.K., Wong, S.H., Liu, D., Kwong, T.N.Y., Nakatsu, G., Yan, P.S., Chuang, Y.M., Chan,
842 M.W.Y., Coker, O.O., et al. (2020). Bacteria pathogens drive host colonic epithelial cell promoter
843 hypermethylation of tumor suppressor genes in colorectal cancer. *Microbiome* 8, 108.
- 844 Xu, J., Yang, M., Wang, D., Zhang, S., Yan, S., Zhu, Y., and Chen, W. (2020). Alteration of the abundance
845 of *Parvimonas micra* in the gut along the adenoma-carcinoma sequence. *Oncol. Lett.* 20, 106.
- 846 Zeller, G., Tap, J., Voigt, A.Y., Sunagawa, S., Kultima, J.R., Costea, P.I., Amiot, A., Böhm, J., Brunetti,

847 F., Habermann, N., et al. (2014). Potential of fecal microbiota for early-stage detection of colorectal
848 cancer. *Mol. Syst. Biol.* *10*, 766.

849 Zhang, L., Anglesio, M.S., O'Sullivan, M., Zhang, F., Yang, G., Sarao, R., Nghiem, M.P., Cronin, S., Hara,
850 H., Melnyk, N., et al. (2007). The E3 ligase HACE1 is a critical chromosome 6q21 tumor suppressor
851 involved in multiple cancers. *Nat. Med.* *13*, 1060–1069.

852 Zhao, L., Zhou, Y., Zhao, R., Coker, O.O.O., Zhang, X., Chu, E.S., Wei, H., Wu, W.K., Wong, S.H., Sung,
853 J.J., et al. (2020). *Parvimonas Micra* Promotes Intestinal Tumorigenesis in Conventional *Apcmin/+* Mice
854 and in Germ-Free Mice. *Research Square* doi:10.21203/RS.3.RS-25974/V1.

855 Zhao, M., Kim, P., Mitra, R., Zhao, J., and Zhao, Z. (2016). TSGene 2.0: An updated literature-based
856 knowledgebase for Tumor Suppressor Genes. *Nucleic Acids Res.* *44*, D1023–D1031.

857 Zhao, M., Liu, Y., Zheng, C., and Qu, H. (2019). dbEMT 2.0: An updated database for epithelial-
858 mesenchymal transition genes with experimentally verified information and precalculated regulation
859 information for cancer metastasis. *J. Genet. Genomics* *46*, 595–597.

860

861

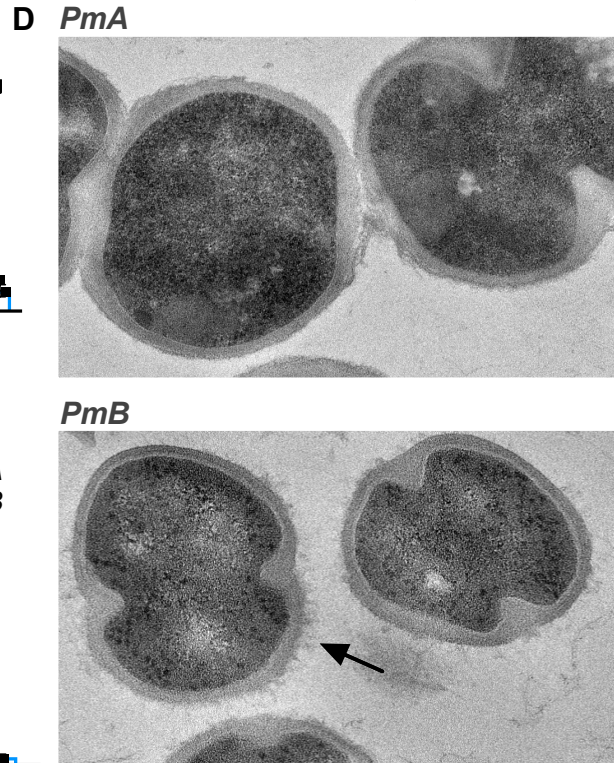
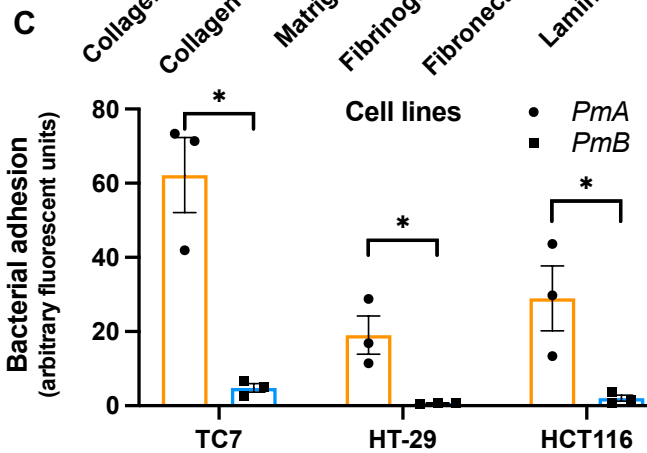
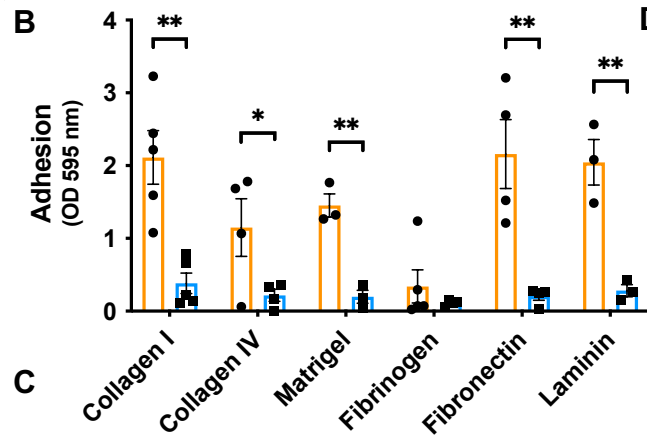
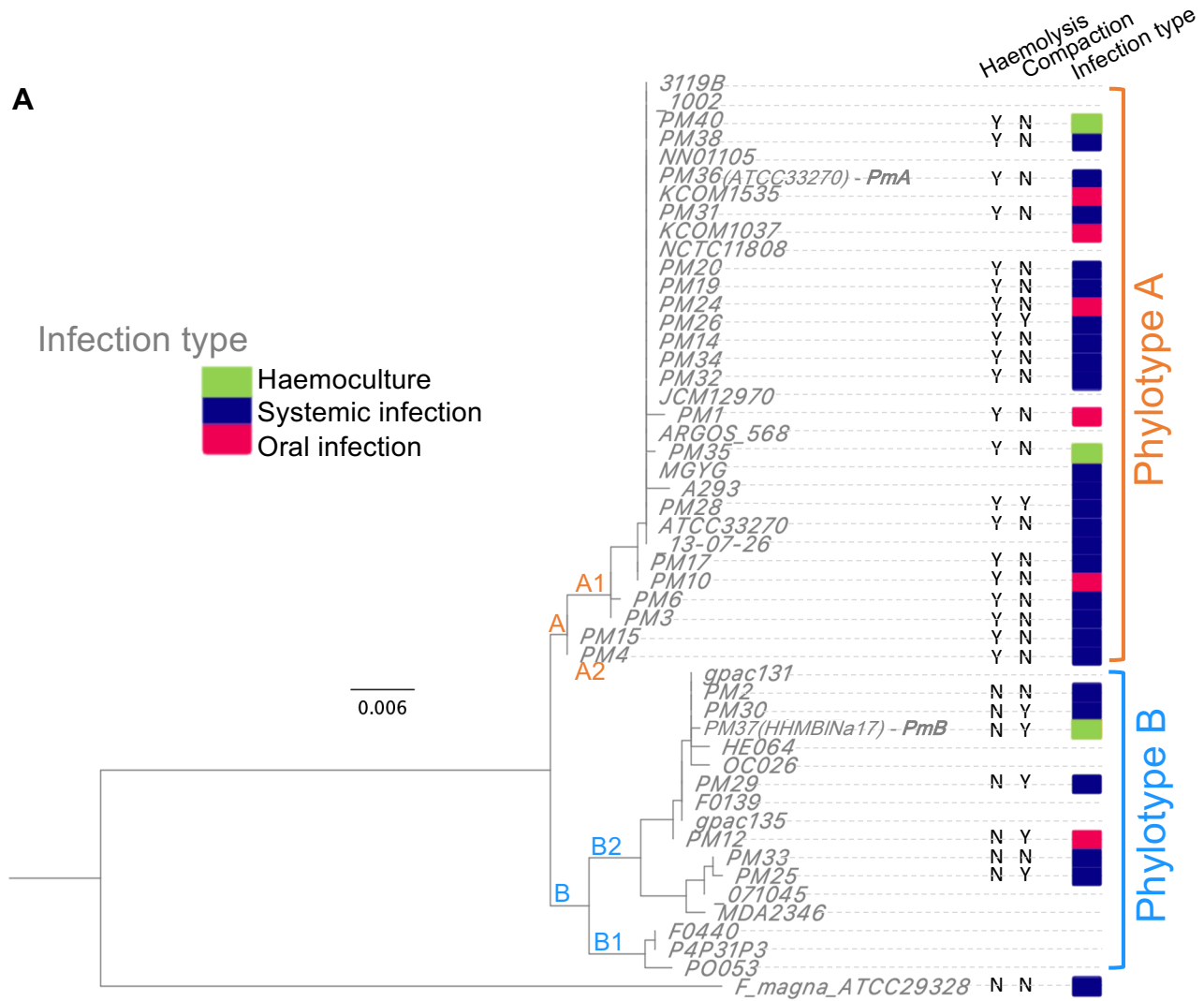


Fig. 1

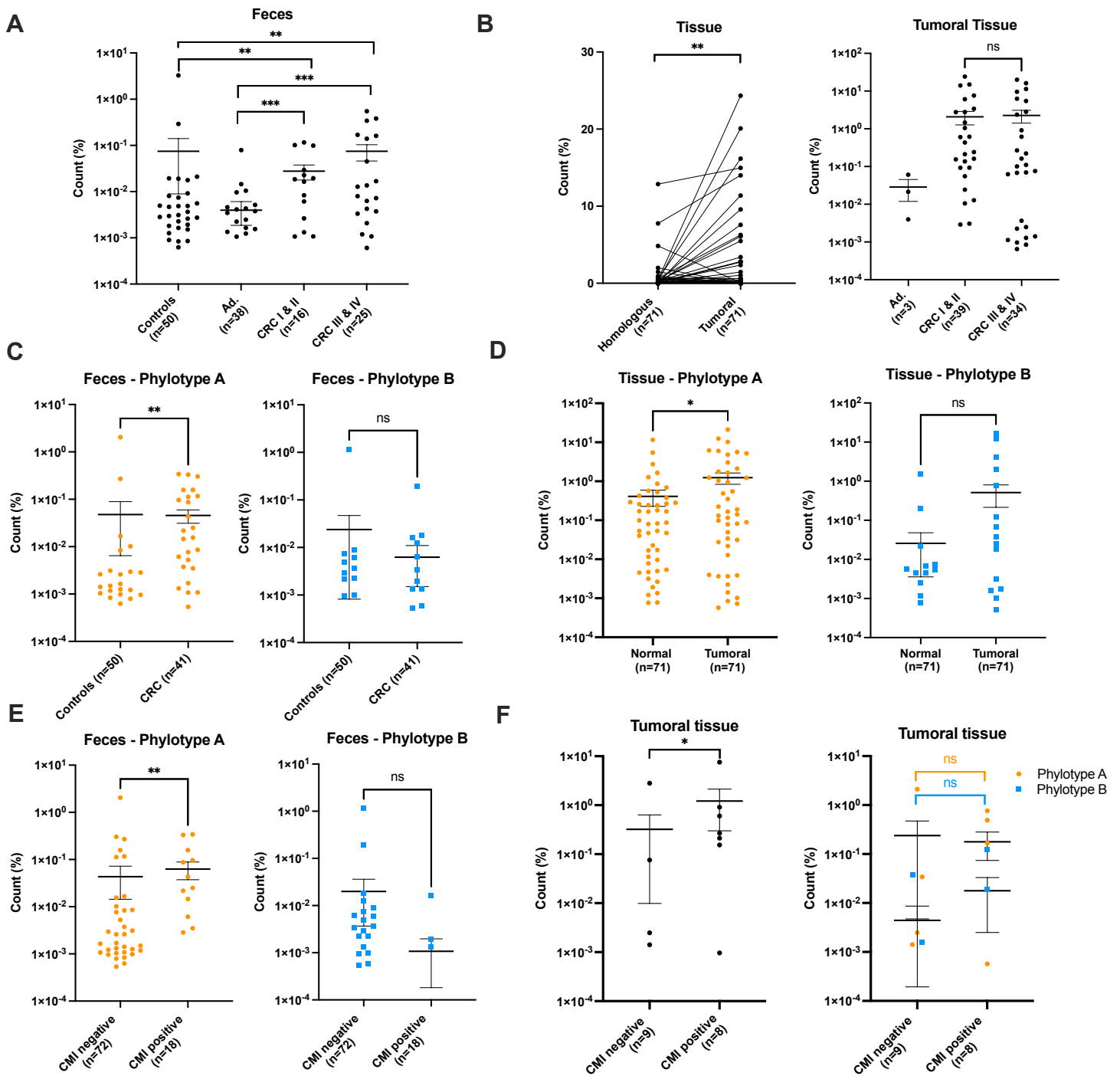


Fig. 2

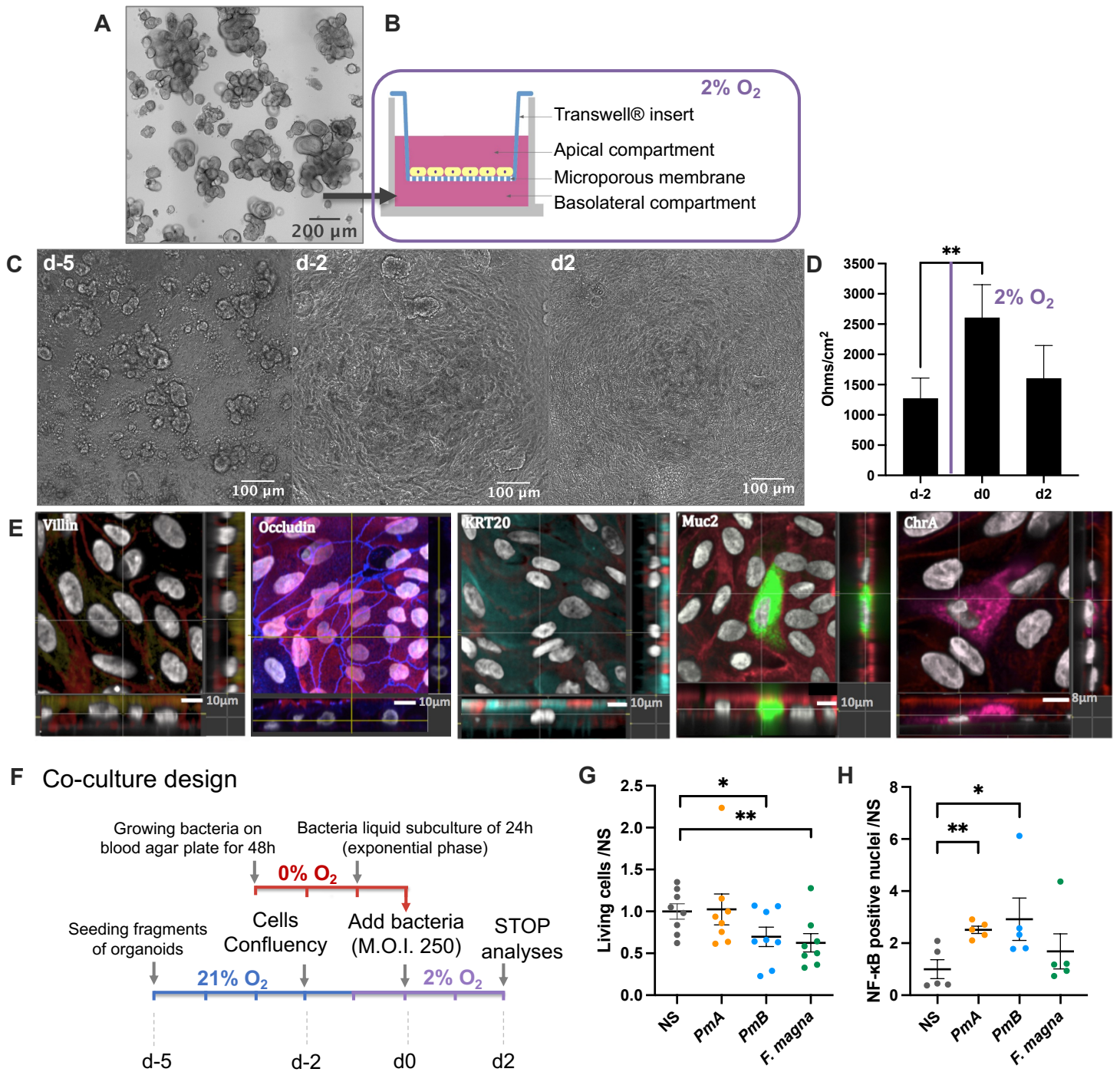
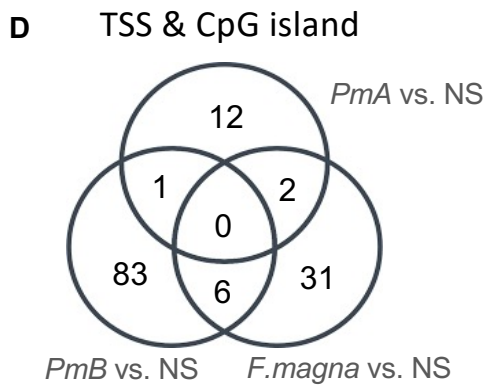
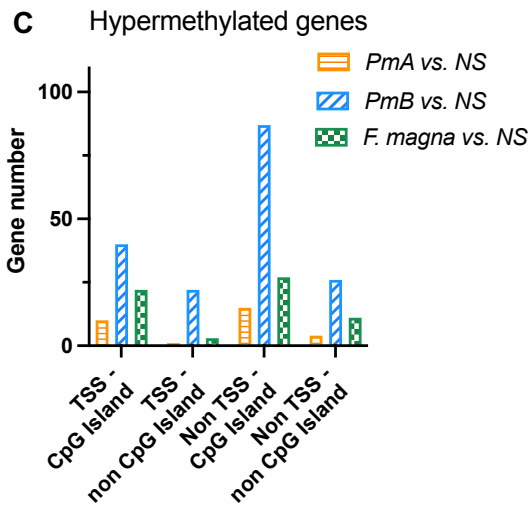
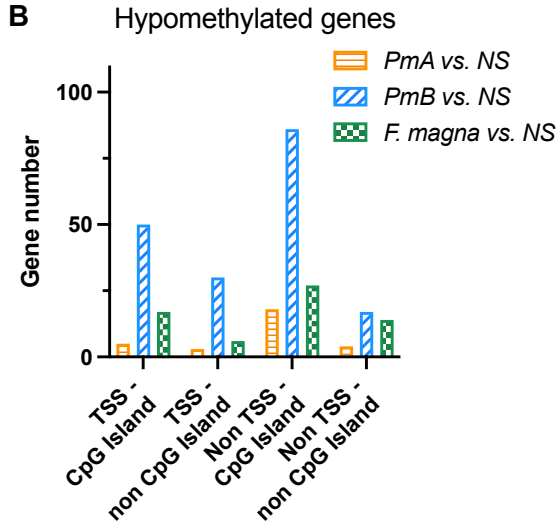
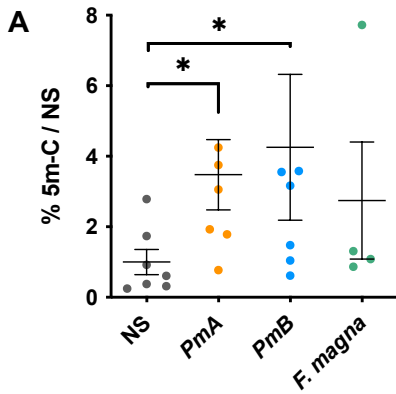


Fig. 3



E Top 15 of differentially methylated gene (TSS & CpG island)

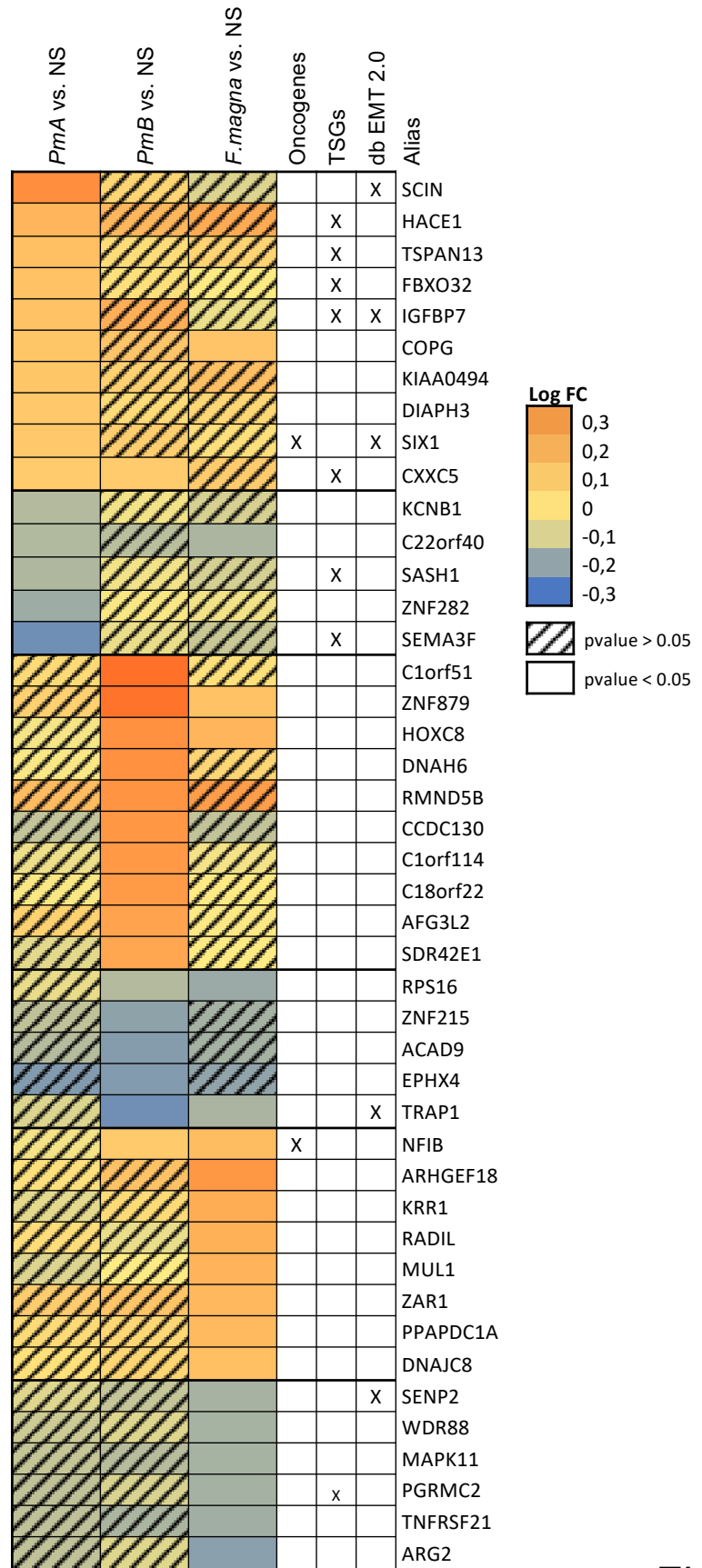


Fig. 4

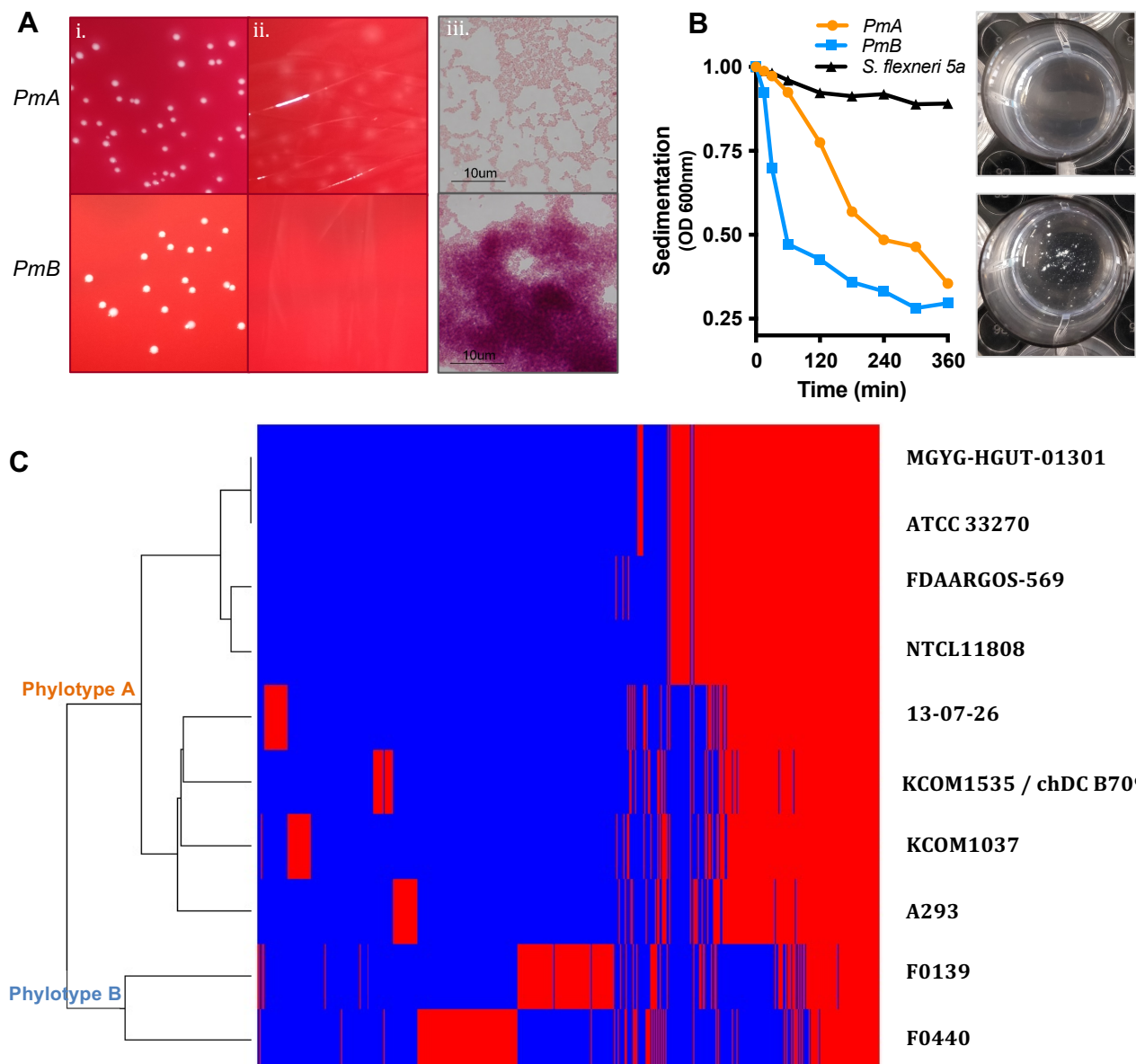


Fig. S1

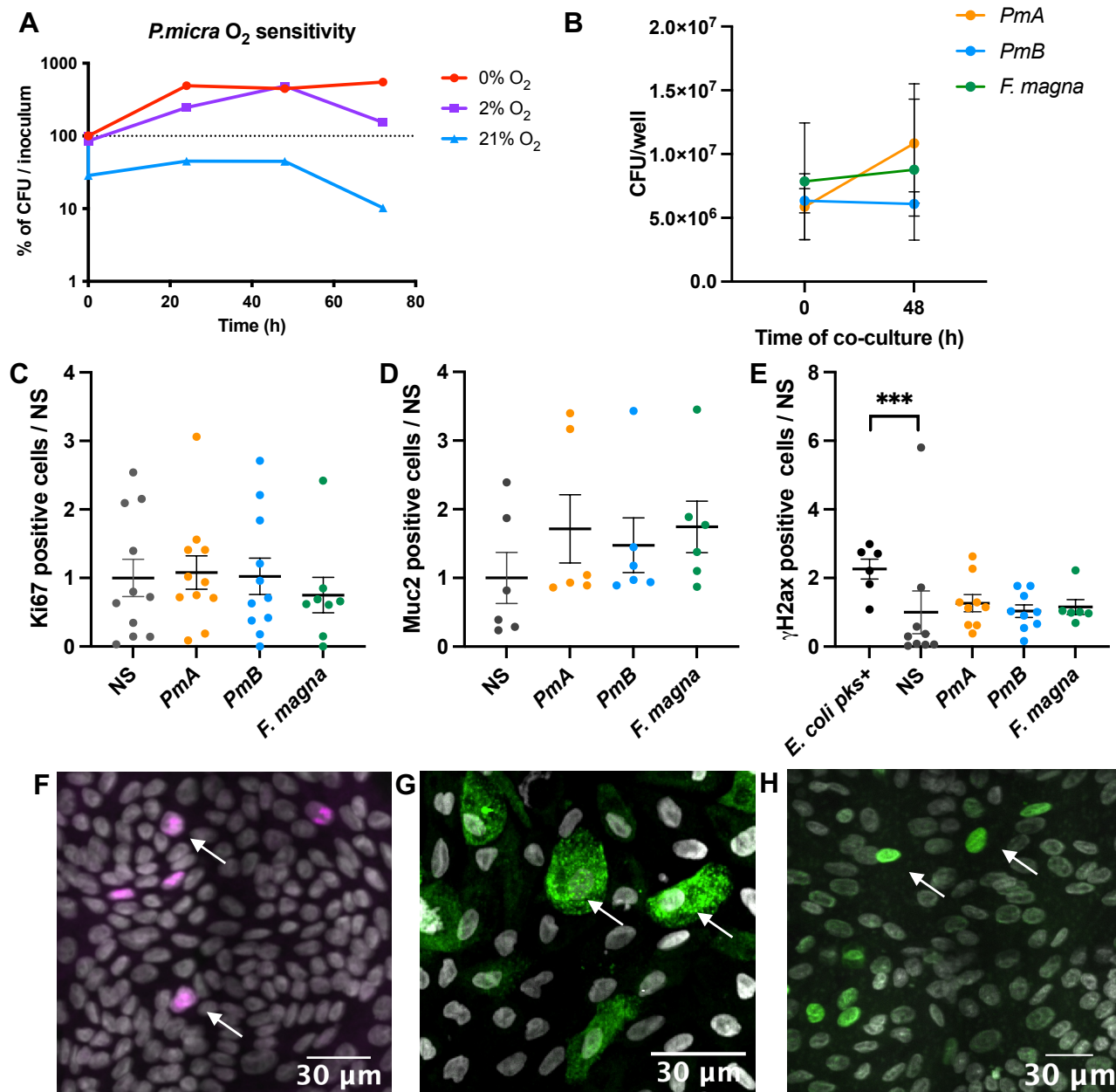


Fig. S2

Clinical isolate number	Origin	Source of isolation	Hemolysis	Colonies compaction	Phylogenetic Group	GenBank accession numbers
PM 1	Pitié Salpêtrière	Dental cellulite	+	-	A1	OM287472
PM 10	Pitié Salpêtrière	Dental cellulite	+	-	A1	OM287474
PM 14	Pitié Salpêtrière	Cerebral abscess	+	-	A1	OM287469
PM 15	Pitié Salpêtrière	Cerebral abscess	+	-	A2	OM287478
PM 17	Pitié Salpêtrière	Cerebral abscess	+	-	A1	OM287473
PM 19	Pitié Salpêtrière	Cervical abscess	+	-	A1	OM287466
PM 20	Pitié Salpêtrière	Cervical adenopathy	+	-	A1	OM287465
PM 24	Pitié Salpêtrière	Lower canaliculus	+	-	A1	OM287467
PM 26	Pitié Salpêtrière	Cerebral abscess	+	+	A1	OM287468
PM 28	Cochin	Femur	+	+	A1	OM287464
PM 3	Pitié Salpêtrière	Cerebral abscess	+	-	A1	OM287476
PM 31	Henri Mondor	Empyema brain abscesses	+	-	A1	OM287463
PM 32	Cochin	Hip articular	+	-	A1	OM287471
PM 34	Cochin	Hip	+	-	A1	OM287470
PM 35	Henri Mondor	Hemoculture	+	-	A1	OM287462
PM 36 / ATCC 33270 / PmA	CIP Pasteur	Purulent pleurisy	+	-	A1	OM287461
PM 38	CIP Pasteur	Abdominal wound	+	-	A1	OM287460
PM 4	Pitié Salpêtrière	Cerebral abscess	+	-	A2	OM287477
PM 40	Henri Mondor	Haemoculture	+	-	A1	OM287459
PM 6	Pitié Salpêtrière	Cerebral abscess	+	-	A1	OM28747
PM 25	Pitié Salpêtrière	Cerebral abscess	-	+	B2a	OM287480
PM 33	Cochin	Knee joint	-	-	B2a	OM287479
PM 12	Pitié Salpêtrière	Maxillary sinus	-	+	B2b	OM287481
PM 2	Pitié Salpêtrière	Cervical collection	-	-	B2b	OM287484
PM 29	Cochin	Urinary tract	-	+	B2b	OM287482
PM 30	Cochin	Femur	-	+	B2b	OM287483
PM 37 / HHM BINA17 / PmB	Henri Mondor	Haemoculture	-	+	B2b	OM287485

Table S1: Description of *P. micra* clinical isolates obtained from several hospitals in Paris and from different infectious locations.

Samples	Feces n= 166	Tissue (tumor and homologous) n=71
<i>Status</i>	Control n= 88; CRC n= 78	CRC n=71
<i>Tumor localization</i>	Right or transversal colon n= 27 Sigmoid or left Colon n= 48, ind=3	Right or transversal colon n= 35 Sigmoid or left Colon n= 41
<i>TNM stages</i>	I or II n= 27; III or IV n= 48, ind=3	I or II n= 40; III or IV n=31
<i>Gender (Female/male)</i>	F: n= 70; M: n= 76	F: n= 23; M: n=48
<i>Ages (mean +/- SEM)</i>	Control: 60.48 +/- 1.13 CRC: 66.23 +/-1.60	CRC: 65.46 +/- 1.22
<i>BMI (kg/m2) mean +/- SEM</i>	Control: 25.18 +/- 0.4 CCR: 25.67 +/- 0.81	CRC: 25.2 +/- 0.5
<i>Cumulative methylation index (Negative/Positive)</i>	N: n= 119; P: n= 43	N: n= 8; P: n= 7

Table S2: Clinical data. Ind, indetermined.

Names, Alias	Described role	Link with CRC or cancers	References
SCIN (Scinderin)	Ca(2+)-dependent actin-severing and capping protein. Regulation of actin cytoskeleton.	Overexpressed in CRC. Inhibits cell proliferation and tumorigenesis.	<i>Lin 2019</i>
HACE1 (HECT domain E3 ubiquitin protein ligase 1)	E3 ubiquitin ligase involved in specific tagging of target proteins, leading to their subcellular localization or proteasomal degradation.	TSG. Down-regulated by DNA methylation in CRC. Loss or knockout of HACE1 enhanced tumor growth, invasion, and metastasis; in contrast, the overexpression of HACE1 can inhibit the development of tumors.	<i>Li 2019</i> <i>Hibi 2008</i>
TSPAN13 (Tetraspanin 13)	Transmembrane signal transduction protein that plays a role in the regulation of cell development, activation, growth, motility and invasion.	TSG. Downregulation inhibits proliferation of CRC cells.	<i>Lou 2017</i>
FBXO32 (F-Box Protein 32) Astogin-1	Component of a SCF E3 ubiquitin-protein ligase complex which mediates the ubiquitination and subsequent proteasomal degradation of target proteins.	TSG. Under-expressed in CRC. Induce cell differentiation. Upstream regulator of EMT.	<i>Yuan 2018</i> <i>Sahy 2017</i>
IGFBP7 (Insulin Like Growth Factor Binding Protein 7)	Protein coding gene that regulate IGFs. Stimulates prostacyclin production and cell adhesion. Promotes cancer cell growth and migration.	TSG. Silencing induce metastasis.	<i>Ruan 2007</i> <i>Suzuki 2010</i>
KIAA0494 (EF-Hand Calcium Binding Domain 14)	Uncharacterized protein. Predicted membrane protein.	-	
DIAPH3 (Diaphanous Related Formin 3)	Protein coding gene involve in actin remodeling. Regulate cell movement and adhesion.	Deficiency enhances cell motility, invasion and metastasis in many cancers.	<i>Hager 2012</i> <i>Rana 2018</i>
SIX1 (six oculis homeobox 1)	Transcription factor involve in regulation of cell proliferation, apoptosis, embryonic development and tumorigenesis.	Oncogene. Overexpressed in CRC, overexpression of Six1 dramatically promotes CRC tumor growth and metastasis in vivo.	<i>Wu 2014</i> <i>Xu 2017</i>
KCNB1 (Potassium Voltage-Gated Channel Subfamily B Member 1)	Voltage-gated potassium channel Kv2.1. Contributes to the pronounced pro-apoptotic potassium current surge during neuronal apoptotic cell death in response to oxidative injury.	KCNB1 polymorphisms correlate to CRC treatment and patient's outcome. Kv2.1 occasionally forms complexes with other voltage-gated potassium alpha-subunits (i.e. Kv9.3), witch its silencing potently inhibiting proliferation in human colon cells.	<i>Li 2015,</i> <i>Fahra 2020</i>
SASH1 (SAM and SH3 domain-containing protein 1)	Scaffold protein involved in the TLR4 signaling. Stimulate cytokine production and endothelial cell migration in response to binding pathogens	TSG. Downregulated in CRC. Downregulation expression was correlated with the formation of metachronous distant metastasis. Loss of SASH1 induces EMT. SASH1 inhibits metastasis formation In Vivo.	<i>Rimkus 2006,</i> <i>Franke 2019</i>
ZNF282 (Zinc Finger Protein 282)	Transcription factor binding the U5RE (U5 repressive element) of HLTV-1 (human T cell leukemia virus type 1) with a repressive effect. Co-activator of the estrogen receptor alpha.	Knockdown reduced migration, invasion and tumorigenesis of ESCC <i>in vitro</i> and reduced the tumorigenicity of ESCC xenograft in nude mouse.	<i>Yeo 2014</i>
SEMA3F (Semaphorin 3F)	Secreted signaling protein that are involved in axon guidance during neuronal development. Act in an autocrine fashion to induce apoptosis, inhibit cell proliferation and survival. Regulator of actin cytoskeleton.	TSG. Down-regulated by DNA methylation in CRC tissues and CRC cell lines. Associated with progressive phenotypes of CRC. Overexpression reduced proliferation, adhesion, and migratory capability of colon cancer cells. SEMA3F-overexpressing cells exhibited diminished tumorigenesis when transplanted in nude mice and reduced liver metastases.	<i>Gao 2015,</i> <i>Wu 2011,</i> <i>Bielenberg 2004</i>

Table S3: *PmA* induces DNA methylation changes in promoters of genes involved in carcinogenesis. CRC: colorectal cancer; TSG: Tumor suppressor gene; EMT: epithelial-mesenchymal transition; IGFs: insulin-like growth factors; SCF: SKP1-CUL1-F-box protein; TRAPP: Transport Protein Particle; ESCC: Esophageal squamous cell carcinoma.